arXiv:1510.00392v1 [astro-ph.SR] 1 Oct 2015

To be submitted to AJ; draft December 21, 2021

High Resolution Imaging of Very Low Mass Spectral Binaries: Three Resolved Systems and Detection of Orbital Motion in an L/T Transition Binary*

Daniella C. Bardalez Gagliuffi[1,2,3], Christopher R. Gelino[2,4], Adam J. Burgasser[1]

ABSTRACT

We present high resolution Laser Guide Star Adaptive Optics imaging of 43 late-M, L and T dwarf systems with Keck/NIRC2. These include 17 spectral binary candidates, systems whose spectra suggest the presence of a T dwarf secondary. We resolve three systems: 2MASS J1341−3052, SDSS J1511+0607 and SDSS J2052−1609; the first two are resolved for the first time. All three have projected separations < 8 AU and estimated periods of $14 - 80$ years. We also report a preliminary orbit determination for SDSS J2052−1609 based on six epochs of resolved astrometry between 2005−2010. Among the 14 unresolved spectral binaries, 5 systems were confirmed binaries but remained unresolved, implying a minimum binary fraction of $47^{+12}_{-11}\%$ for this sample. Our inability to resolve most of the spectral binaries, including the confirmed binaries, supports the hypothesis that a large fraction of very low mass systems have relatively small separations and are missed with direct imaging.

Subject headings: stars: binaries: general — stars: fundamental parameters — stars: individual (2MASS J13411160−30525049, SDSS J151114.66+060742.9, SDSS J205235.31−160929.8) — stars: low mass, brown dwarfs

1. Introduction

Observational studies of field brown dwarfs indicate that only $\sim 10 - 20\%$ are found in very low mass (VLM) binary systems (Bouy et al. 2003; Close et al. 2003; Basri & Reiners 2006; Allen 2007; Burgasser 2007a; Kraus & Hillenbrand 2012). In contrast, the binary fraction for G stars is $\sim 40\%$ (Duquennoy & Mayor 1991) and $\sim 30\%$ for M dwarfs (Fischer & Marcy 1992). These statistics suggest a steady decline of binary fraction with mass. The peak in the observed projected separation distribution also decreases with mass, going from 30AU for G dwarfs (Duquennoy & Mayor 1991), $4 - 30$AU for M dwarfs (Raghavan et al. 2010; Fischer & Marcy 1992) to $6 - 8$AU for VLM stars and brown dwarfs (Allen 2007; Burgasser et al. 2007; Kraus & Hillenbrand 2012).

[1]Center for Astrophysics and Space Sciences, University of California, San Diego, 9500 Gilman Dr., Mail Code 0424, La Jolla, CA 92093, USA.

[2]Infrared Processing and Analysis Center, California Institute of Technology, Pasadena, CA 91125, USA.

[3]IPAC Visiting Graduate Student Fellow 2014.

[4]NASA Exoplanet Science Institute, California Institute of Technology, Pasadena, CA 91125.

*Some of the data presented herein were obtained at the W.M. Keck Observatory, which is operated as a scientific partnership among the California Institute of Technology, the University of California, and the National Aeronautics and Space Administration. The Observatory was made possible by the generous financial support of the W.M. Keck Foundation.

The observed peak in the projected separation distribution for VLM dwarfs is largely based on direct imaging studies, which have discovered > 80% of the VLM binary systems to date (Burgasser et al. 2007; Bardalez Gagliuffi et al. 2014 [hereafter: BG14]). Angular resolution limits impose a bias on the separations observed. For ground-based telescopes with Adaptive Optics (AO) and the Hubble Space Telescope (HST), this resolution limit is roughly $0\farcs05 - 0\farcs1$, which at the typical distances of known VLM dwarfs, $20 - 40$pc[1], corresponds to the observed peak in the projected separation distribution. Tighter systems are unresolvable. Measurements of radial velocity (RV) and astrometric variability more adequately probe the small projected separation regime, but such measurements are resource-intensive and introduce their own set of geometric biases. An alternative approach to identifying closely-separated VLM binaries is as *spectral binary* systems. Spectral binaries exhibit peculiarities in blended-light spectra that arise from the superposition of two components with distinct spectral morphologies. This method has been used to disentangle the spectra of white dwarf/M dwarf binaries (Silvestri et al. 2007) and more recently, VLM stars and brown dwarfs, especially those with a T dwarf component (e.g. Cruz et al. 2004; Metchev et al. 2008; Burgasser et al. 2010 [hereafter: B10]; Geißler et al. 2011; Day-Jones et al. 2013; BG14). The identification of spectral binaries is independent of their projected separation, allowing the identification of binaries with very tight separations. The selection biases for this method (small separation, distinct component masses) are different from those of direct imaging, RV and astrometric variability, and overluminosity, providing a complementary approach to finding VLM binary systems.

While many brown dwarf spectral binaries have been discovered serendipitously (Cruz et al. 2004; Burgasser 2007b; Gelino & Burgasser 2010), recent systematic searches (B10, BG14) have increased the number of known spectral binaries to ∼50. Follow-up of candidates is necessary to confirm their binary nature since the spectral peculiarities that signal binarity may instead be the result of atmospheric variability, as in the case of the T1.5 2MASS J21392676+0220226[2] (Radigan et al. 2012; Khandrika et al. 2013). Only 12 spectral binaries have been confirmed by direct imaging, radial velocity, astrometric variability or overluminosity (See Table 8; Burgasser et al. 2006b; Blake et al. 2008; Gelino & Burgasser 2010; Burgasser et al. 2011b; Stumpf et al. 2011; Burgasser et al. 2012; Dupuy & Liu 2012; Faherty et al. 2012; Manjavacas et al. 2013) and many of these have turned out to be close separation systems. The M9 dwarf SDSS J0006−0852AB (Burgasser et al. 2012) and the M8.5 dwarf 2MASS J0320−0446AB (Blake et al. 2008; Burgasser et al. 2008) were confirmed as binaries by RV variability and found to have projected separations < 1AU. The L4 dwarf SDSS J0805+4812 (Burgasser 2007b), confirmed as a binary through astrometric variability, has a semi-major axis $0.9 - 2.3$AU (Dupuy & Liu 2012). Even with the high resolution images provided by the Keck II Laser Guide Star Adaptive Optics (LGS-AO) system, none of these binaries can be resolved.

Nevertheless, high resolution imaging remains an efficient first test for binarity. In this article, we present high resolution LGS-AO observations of 43 late-M, L and T dwarfs, 17 of which are spectral binary candidates. Section 2 describes the target selection and observation procedures using the LGS-AO system and Keck II/NIRC2 (van Dam et al. 2006; Wizinowich et al. 2006). For the unresolved spectral binaries (visual and index-selected) we determine detection and separation limits in Section 3.1. We discuss in detail each of the known, unresolved binaries in Section 3.2. We report three resolved sources and describe their properties in Section 3.3. In Section 4.1 we analyze multi-epoch AO images of SDSS J2052−1609 and

[1]In order to achieve S/N≳25 with low and high resolution spectroscopy.

[2]Hereafter targets observed in this study are referred to by shorthand notation: J*hhmm* + *ddmm*, where *h* is hour, *d* is degree and *m* is minute. Full coordinates are listed in Table 1.

determine a first astrometric orbit for this L/T transition system. For the other two resolved systems, we estimate orbital parameters with Monte Carlo methods in Section 4.2. We discuss the broader implications of our results in the context of small separation VLM binaries in Section 4.3. Our results are summarized in Section 5.

2. Target Selection and Observations

2.1. Spectral Binary Identification

The 43 sources observed in our study (Table 1) were selected from known late-M, L and T dwarfs in the vicinity of the Sun with a suitable tip-tilt star for LGS-AO correction. These include 33 M9-T3 dwarfs initially classified as spectral binaries by visual inspection, before the B10 and BG14 selection criteria had been defined. We re-examined their binary candidacy by dividing them into two groups according to spectral type: 15 objects in the M7-L7 range analyzed with the BG14 method, and 22 objects in the L5-T3 range, analyzed with the B10 method. The four objects overlapping in these spectral type ranges were analyzed by both methods. Ten other low mass stars and brown dwarfs were also observed as back-up targets, but were excluded from the analysis because visual inspection rejected them as spectral binary candidates.

Indices were measured from low resolution ($\lambda/\Delta\lambda = 75-120$), near-infrared IRTF/SpeX spectra (Rayner et al. 2003) covering $0.9 - 2.4\mu$m, accessed from the SpeX Prism Libraries (Burgasser 2014). One of our targets, 2MASS J2126+7617, has a declination outside the observable range of SpeX/IRTF ($-50^\circ < \delta < +67^\circ$), so a smoothed Keck/NIRSPEC spectrum was used instead (Kirkpatrick et al. 2010). Spectral indices given in B10 and BG14 were calculated for each spectrum, and regions of interest (ROI) in index-index spaces were delineated using confirmed binaries. Slight modifications to the limits of some ROIs in both B10 and BG14 were made to include known binaries WISEP J0720−0846 and 2MASS J1209−1004 (Burgasser et al. 2015b; Liu et al. 2010, respectively), which had not been detected at the time the index selection criteria were defined. Table 2 shows the updated limits of the index selection ROIs for both sets of criteria. Strong and weak candidates are selected by the number of times they fall within the ROIs, as described in B10 and BG14.

From the BG14 set, 8 sources were selected as candidates from spectral indices (4 as strong, 4 as weak). Single and binary templates were fit to these index-selected sources, ranked by a χ^2 statistic. The best fit single and binary templates were compared to each other with an F-test to assess the percentage confidence that the binary fit is statistically better than the single fit. The primary types were constrained to ±3 subtypes from the combined optical spectral type or, in its absence, near infrared type, and the secondary types were allowed to vary between T1 and T8. After template fitting, 6 sources remained as candidates. From the B10 set, 16 sources were selected as index candidates (11 as strong, 5 as weak) and after fitting, 12 sources remained as candidates. 2MASS J1711+2232 was selected as a candidate on both sets. In all, we classify 17 sources as true spectral binary candidates (Table 1), close to half of the visually-selected spectral binaries.

2.2. NIRC2 High Resolution Imaging and Reduction

High angular resolution images of our targets were obtained using the Keck II LGS-AO system with NIRC2 on nine nights between August 2009 and January 2014. Tip-tilt reference stars within $60''$ of the

targets were selected from the USNO-B catalog (Monet et al. 2003). A 3-point dither pattern was used to avoid the noisy lower left quadrant of the array, and was repeated as needed with different dither offsets to build up long exposures. Total integration times were between 60s and 720s, depending on the brightness of the source and the atmospheric conditions. All objects were observed with the Mauna Kea Observatories (MKO) H filter (Simons & Tokunaga 2002; Tokunaga et al. 2002) and narrow plate scale (9.970±0.012 mas/pixel for a single-frame field-of-view of $10'' \times 10''$; Pravdo et al. 2006). The MKO J and/or K_s filters were also used for targets with apparent companions.

The images were reduced in a standard fashion using Interactive Data Language (IDL) scripts. First, a dark frame was subtracted from each science frame. For each science exposure a sky frame was constructed from the median average of all images acquired for the target, exclusive of the frame being reduced. The sky-subtracted frames were then divided by a normalized dome flat. A bad pixel mask was applied to smooth over bad pixels using the average of the neighboring pixels. All images in a given epoch and common filter were shifted to align the target to a common location, and the stack was median-combined to create the final mosaics.

3. Analysis

3.1. Image Characterization and Companion Detection Limits for Unresolved Sources

The reduced image mosaics around each target are shown in Figures 1 and 2. Strehl and signal-to-noise ratios (S/N) are reported in Table 1. The Strehl ratio was calculated by comparing each point source to a theoretical, diffraction-limited, monochromatic, NIRC2 point spread function (PSF) with the `NIRC2Strehl` IDL routine[3]. The S/N was computed assuming Poisson statistics:

$$S/N = \frac{N_{star}}{\sqrt{n_{sky}\ \sigma_{sky}^2 + \frac{N_{star}}{g}}} \tag{1}$$

where N_{star} is the total counts from the star at a radius of 1.5 times the full width at half maximum, n_{sky} is the number of pixels used for the standard deviation of the sky counts, σ_{sky}, which encompasses noise from several sources (read out, dark current, image reduction, etc.) and g is the gain in DN/e^- (data number per electron).

Three of our sources are resolved: 2MASS 1341−3052, SDSS 1511+0607 and SDSS 2052−1609; these are shown in Figure 1 and discussed further in Section 3.3. One source, 2MASS J1733−1654, has a feature that we cannot distinguish between bona fide source and PSF structure, so we consider this to be a "source of interest". The remaining sources are unresolved at the limits of our sensitivity and image quality. Because the PSF of the images vary considerably, we determined detection limits through a source implantation simulation of representative images. We organized the targets by Strehl and S/N and selected two representative sources of high Strehl (WISE J0047+6308) and low Strehl (2MASS J0032+0219), as shown in Figure 3. For these sources, we simulated binary companions by scaling down the brightness of each image, and then shifting and superimposing it onto the original image. The implanted image was scaled down by a maximum of 6 magnitudes, which was the largest magnitude difference inferred from the template fitting of spectral binary candidates, and shifted by up to 50 pixels or $\sim 0\farcs5$ in any angle. Magnitude difference, separation and position angle were all drawn from a uniform random distribution.

[3]Retrieved from `https://www2.keck.hawaii.edu/optics/lgsao/software/`

We visually examined each image at multiple contrast ratios to search for the implanted companion. This experiment was performed N$\gtrsim$12,000 times per source, varying the target, scale factor and offset. A "detection" required clicking within 15 pixels of the implanted secondary, with the option to decide if an implanted companion was visually undetectable. We determined the maximum relative magnitude as a function of separation for which the detection fraction exceeded 50%. The detection fraction was calculated in steps of 0.5 mag and 0.″05, sliding by half a step along both axes for a total of ∼400 overlapping bins. Figure 4 shows that the PSF dominates the sensitivity close to the star centroid. For the case of low Strehl ratio, detections reach a minimum at $\Delta H \approx 5$ mag, 0.″3 away from the center of the PSF, beyond which our sensitivity is limited by sky noise. For the high Strehl ratio case the floor lies around 5.5 magnitude difference at radii greater than 0.″4.

We applied the sensitivity curves of our representative sources to systems with similar Strehl ratios. For the 30 unresolved spectral binary candidates, we compared these sensitivity limits to the magnitude differences predicted from template fitting to determine separation limits (Table 3). Figure 5 shows an example of the sensitivity curve and separation constraint for the spectral binary candidate 2MASS J1711+2232. Five of our unresolved spectral binaries have been previously confirmed as true binaries (See Section 3.2), but our separation limits are up to 40% greater, i.e. these binaries can not be resolved with our observations. For the case of 2MASS J1209-1004, our estimated separation limit is smaller than the measured separation, suggesting that the secondary has moved to a closer configuration. Similarly, for our three resolved systems the calculated separation limit is always smaller than the measured separation, which means that our separation limits correctly constrain the PSF of the primary. The remaining 9 unresolved spectral binaries have angular separation limits between 0.″04 − 0.″28.

3.2. Unresolved Known Binaries

3.2.1. 2MASS J05185995-2828372

2MASS J0518−2828 was the first source to be identified as a spectral binary of L6 and T4 components (Cruz et al. 2004) and was marginally resolved with HST (Burgasser et al. 2006b) with an angular separation of 0.″051 ± 0.″012. Dupuy & Liu (2012) find a small astrometric perturbation for this source that cannot be clearly attributed to orbital motion. Konopacky et al. (2010) observed this source with LGS-AO at Keck in 2006 and were not able to resolve it. Its parallactic distance has been measured to be 22.9±0.4 pc (Dupuy & Liu 2012), implying a projected separation of 1.17±0.28 AU from the HST measurement. Our LGS-AO observations also fail to resolve this system to a limit of 98 *mas* or 2.2 AU, which is consistent with the HST observations. This system appears to be a very tight binary whose separation is just below the limits of ground-based AO imaging.

3.2.2. WISEP J072003.20−084651.2

WISEP J0720−0846 was discovered by Scholz (2014) and confirmed by Burgasser et al. (2015b) as an M9 at a distance of 6.0±1.0 pc. The latter study identified a candidate companion at an angular separation of 139±14 *mas* in NIRC2 LGS-AO observations, which has been confirmed at a slightly wider offset (angular separation 197 ± 3 *mas*, projected separation 1.18 ± 0.21AU) with $\Delta H = 3.85 \pm 0.11$ mag in follow-up observations (Burgasser et al. 2015a). Our analysis does not resolve the companion to limits of 500 *mas* and 3 AU, beyond the separation reported in that study.

3.2.3. SDSS J080531.84+481233.0

SDSS J0805+4812 is a blue L dwarf discovered by Hawley et al. (2002), and a spectral binary of L4.5 and T5 components (Burgasser 2007b). This source shows astrometric variability with an amplitude of 15 *mas* (Dupuy & Liu 2012). Our LGS-AO observations show an elongated PSF that we attribute to tip-tilt correction errors, but no resolved companion. Dupuy & Liu (2012) estimate a semi-major axis of $40-100\,mas$ assuming a mass ratio $q = 0.55 - 0.88$ and from the measured parallactic distance of 22.9 ± 0.6pc, they infer a projected separation of $0.9 - 2.3$AU. Our observations do not resolve this system to limits of 164 *mas* and 3.8 AU, both consistent with the Dupuy & Liu (2012) estimates.

3.2.4. 2MASS J11061197+2754225

The T2.5 2MASS J1106+2754 was first discovered by Looper et al. (2007) and later observed with NIRC2 with LGS-AO in June 2006, but was unresolved (Looper et al. 2008b). B10 identified it as a spectral binary of T0.0±0.2 and T4.5±0.2 components due to its CH_4 absorption feature in the H band, and ruled out a separation greater than 1.5 AU based on Keck imaging. Manjavacas et al. (2013) finds that this source is ∼1 mag overluminous and determined a parallactic distance of $20.6^{+1.0}_{-1.2}$ pc. Our LGS-AO observations were unable to resolve this source, implying upper limits of 74 *mas* and 1.5 AU, the same constraint as that reported by Burgasser et al. (2010).

3.2.5. 2MASS J12095613-1004008

2MASS J1209−1004 was first discovered by Burgasser et al. (2004) and is the T3 spectral standard (Burgasser et al. 2006a). Liu et al. (2010) resolved the system with NIRC2 and LGS-AO in the J band, and estimated component types of T2.0±0.5 and T7.5±0.5 based on photometry. The mass ratio of this binary is estimated to be $q = 0.5$, which is unusually small for brown dwarf binaries (Bouy et al. 2003; Burgasser 2007a). Liu et al. (2010) found an angular separation of 151 ± 13 *mas* at a position angle of $314° \pm 5°$ with a magnitude difference of $\Delta H = 2.8 \pm 0.3$ mag. Its parallactic distance $d = 21.8$±0.5 pc (Dupuy & Liu 2012) leads to a projected separation of 3.3±0.3 AU. This source was not resolved in our H band LGS-AO image, with limits of 95 *mas* and 2.1 AU. In this case, our observation should have detected the companion, suggesting that orbital motion may have moved into closer projected alignment, or that the companion could be the source of the elongation of the PSF to the South East.

3.3. Resolved Binaries

3.3.1. 2MASS J13411160−30525049

The L3 2MASS 1341−3052 was first discovered by Reid et al. (2008) in the Two Micron All Sky Survey (2MASS; Cutri et al. 2003) and later identified as a spectral binary candidate with L1.0±0.5 and T6.0±1.0 components (BG14). Our NIRC2 observations resolve the source with an angular separation of $279 \pm 17\,mas$ at a position angle of $317.9° \pm 0.6°$. The original template matching analysis assumed relative spectral fluxes on the Looper et al. (2008a) absolute magnitude to spectral type relation. We repeated this analysis using the relative photometry in all three JHK_s bands to scale and select binary templates in a similar fashion as

described in Burgasser et al. (2011a). Our revised template fit analysis resulted in component spectral types of L2.5±1.0 and T6.0±1.0; i.e. we infer a primary classification more consistent with the combined-light optical classification.

2MASS J1341−3052 is the only one of the three resolved systems that does not have a parallax measurement. We estimated its distance using the calculated component apparent magnitudes with the Dupuy & Liu (2012) spectral type to absolute magnitude relation and component spectral types from template fitting. Uncertainties were propagated from spectral type, apparent magnitudes and spectral type relation, accordingly. We calculated one distance per filter and then obtained the weighted average distance from the MKO JHK_s filters. The distances for both components (29±3 pc for the primary and 31±6 pc for the secondary were consistent across filters. The uncertainty-weighted average yields a distance estimate of 29±3 pc. From this we infer a projected separation of 8.1 ± 0.5 AU.

A spectral type versus absolute magnitude plot is shown in Figure 6, using the Dupuy & Liu (2012) parallax sample of 259 objects as a reference. The primary absolute magnitude is anchored to the Dupuy & Liu (2012) relation due to the lack of a trigonometric distance, while the secondary absolute magnitude was derived from the primary's using the measured relative magnitude. In the J band, the secondary adds 0.09 mags to the primary, barely enough to make the combined absolute magnitude look like an outlier. In the K band, the secondary adds 0.02 mags to the primary, so it appears as if the secondary absolute magnitude also falls on the relation and the combined magnitude is within the $+1\sigma$ curve. This source could not have been detected as an overluminous binary candidate because of the late type of the secondary.

3.3.2. SDSS J151114.66+060742.9

The T0 SDSS J1511+0607 was discovered by Chiu et al. (2006) in the Sloan Digital Sky Survey (SDSS; Adelman-McCarthy et al. 2007). This source was identified as a "strong" binary candidate in B10, and found to be 1 mag overluminous for its spectral type in M_{JHK} by Faherty et al. (2012). Multi-band imaging with NIRC2 on 2009 Aug 15 resolved the system into two components separated by 108 ± 11 *mas* at a position angle of $335° \pm 4°$. The parallax measurement of 37±7 *mas* by Faherty et al. (2012) implies a distance of 28±5 pc, which in turn corresponds to a projected separation of 2.9±0.3 AU. Including the measured relative JHK_s magnitudes in our template fitting gives updated component spectral types of L5.0±1.0 and T5.0±0.5.

Using the combined light magnitude, the relative magnitudes and the parallactic distance, we determined the absolute magnitudes for the components (Figure 6). While the combined absolute magnitude of SDSS J1511+0607 clearly stands out as an outlier in spectral type to absolute magnitude plots, its components look typical. Indeed, its primary lies slightly below the Dupuy & Liu (2012) spectral type to absolute magnitude relation.

3.3.3. SDSS J205235.31−160929.8

Also discovered by Chiu et al. (2006), SDSS 2052−1609 was classified as an T1±1 brown dwarf. B10 identified it as a spectral binary candidate with component types of L7.5±1.0 and T2±0.5, noting that the best fit primary was unusually blue when compared to the median $J - K_s$ colors of Faherty et al. (2009). Stumpf et al. (2011) was able to resolve the components with VLT/NACO, and also reported

archival HST/NICMOS data which confirmed common proper motion and indicated some orbital motion. Stumpf et al. (2011) determined component spectral types by comparing the objects' JHK_s colors to mean colors from Dwarf Archives[4] and obtained divergent results for the primary component (T0.5±0.5 and T2.5±0.5) as compared to those from B10. Using our NIRC2 photometry to constrain spectral template fitting, we find component spectral types of L6.0±2.0 and T2.0±0.5. Dupuy & Liu (2012) find a parallactic distance of 29.5±0.7 pc. The angular separation between the components was measured to be 103±2 *mas*, leading to a projected separation of 3.0±0.1 AU.

Absolute magnitudes of this source and its components were calculated from its parallactic distance and measured magnitude differences. As for the case of SDSS J1511+0607, the primary of SDSS J2052−1609 appears to be underluminous, while its secondary falls comfortably within 1σ from the Dupuy & Liu (2012) relation (Figure 6).

4. Discussion

4.1. A Preliminary Orbit for SDSS J2052−1609AB

Our observations of SDSS J2052−1609AB confirm prior results by Stumpf et al. (2011) and adds to coverage of its orbital motion first detected in that study. We identified additional archival NIRC2 + LGSAO images of the system taken on 2005 October 11, 2007 April 23 (PI M. Liu) and 2010 May 1 (PI B. Biller), and analyzed these data in the same manner as described above. The resulting six epochs of relative astrometry spanning just over 4.5 yr are listed in Table 5 and displayed in Figure 7. These measurements confirm the direction of motion previously identified and cover a significant fraction of the system's orbit.

To more tightly constrain the orbit of this system, we used an Markov Chain Monte Carlo (MCMC) routine with Metropolis-Hasting algorithm (Metropolis et al. 1953; Hastings 1970) to iteratively fit a seven-parameter orbit model to the twelve astrometric measurements (six each in relative Right Ascension and declination) and parallax distance measurement (d = 29.5±0.7 pc; Dupuy & Liu 2012). The methodology used is described in detail in Burgasser et al. (2015a). The parameter vector is

$$\vec{\theta} = (P, a, e, i, \omega, \Omega, M_0, d) \tag{2}$$

where P is the period of the orbit in years, a the semi-major axis in AU, e the eccentricity, i the inclination, ω the argument of periastron, Ω the longitude of nodes, M_0 the mean anomaly at epoch τ_0 = 2453654.31 (Julian Date), and d is the distance in pc. We computed an MCMC chain of 10^7 parameter sets, at each step varying parameters using a normal distribution with scale factors that were allowed to vary dynamically to improve convergence.[5] We applied additional constraints of 1 yr $< P <$ 100 yr and $0 < e < 0.6$ to eliminate improbable regions of parameter space, and constained the distance to lie within 28 pc $< d <$ 31 pc; our parameter chain was largely insensitive to these limits. Convergence of the chain was monitored through autocorrelation of parameters and evolution of divergence in sequential subchains, and acceptance rates were typically 0.5–1%. The first 10% of the MCMC chain was removed from subsequent analysis.

Figure 7 shows the best-fit relative visual orbit compared to the measurements, which is an acceptable

[4]`http://www.dwarfarchives.org`

[5]We used an initial scale factor set $\vec{\beta}$ = (5 yr, 0.5 AU, 0.2, 20°, 20°, 20°, 20°, 0.7 pc), but if a parameter θ_j did not change in 1000 iterations, β_j was changed to 3 times the standard deviation of the previous (up to 100) changed values.

fit ($\chi^2 = 12.05$ for 6 degrees of freedom). Table 6 lists the best-fit orbital parameters, as well as median values and 16% and 84% quartiles, while Figure 8 displays the distributions and correlations of P, a, e, i and $M_{tot} = a^3/P^2$, the total system mass in Solar units. All of the parameters are reasonably well-determined despite the limited phase coverage, although there are strong correlations between P, a, i and e and a hint of a secondary solution (double-peaked distributions). From the primary solution, we estimate an orbit period of 33^{+4}_{-2} yr and total system mass of $0.0823^{+0.0037}_{-0.0017}$ $M_\odot$, which is consistent with the lower limit of 0.074 $M_\odot$ proposed by Stumpf et al. (2011) assuming a circular orbit. Indeed, the orbit of SDSS J2052−1609AB appears to be fairly circular ($0.014^{+0.023}_{-0.010}$) and significantly inclined to the line of sight ($45^{\circ}{}^{+4^{\circ}}_{-2^{\circ}}$). The best fit template fitting results suggest component spectral types of L5.8±1.8 and T2.1±0.5. Assuming effective temperatures corresponding to these spectral types (1544±181K for the primary and 1248±101K for the secondary; Stephens et al. 2009), and using the evolutionary models of Saumon & Marley (2008) to estimate age-dependent component masses, we estimate an age of 0.4–1.4 Gyr for this system, where the range accounts for the total mass uncertainty, effective temperature uncertainties, and cloud effects on brown dwarf evolution. Observations over the next decade should greatly improve the mass and orbit constraints on this system, and resolved spectroscopy should make it possible to critically test evolutionary models (e.g., Konopacky et al. 2010; Dupuy et al. 2014).

4.2. Estimated orbital parameters for 2MASS J1341−3052 and SDSS J1511+0607

For 2MASS J1341−3052 and SDSS J1511+0607 only a single epoch of astrometry is available. Hence, we performed a simple Monte Carlo simulation to find the distributions of likely semi-major axes and periods for these systems. Following the procedure described in Burgasser et al. (2015b), we created random uniformly-distributed vectors for eccentricity $0 < \epsilon < 0.6$ (Dupuy & Liu 2011), inclination $0 < \sin i < 1$, longitude of ascending node $0 < \Omega < 2\pi$, argument of periapse $0 < \omega < 2\pi$, and mean anomaly angle $0 < M < 2\pi$ for 10^5 hypothetical orbits with a fixed semi-major axis of $a = 1$ AU. We numerically solved the Kepler equation to find the eccentric anomaly, calculated the Thiele-Innes constants (Innes 1907; van den Bos 1927), and found the x and y projected positions on the sky leading to the total projected separation, r_{tot}. The distributions of semi-major axes for the resolved systems were inferred by transforming variables:

$$a = (1\text{AU}) \times \frac{\rho d}{r_{tot}} \tag{3}$$

where a is the semi-major axis in AU, ρ is the angular separation in arc seconds, d is the distance to the system in parsecs and r_{tot} is in AU. The observed projected separation, $r_{obs} = \rho d$, constrains the array of allowed orbits, r_{tot}, and as a result we arrive at a distribution of probable semi-major axes, a.

The cumulative probability distributions for the semi-major axes of 2MASS J1341−3052 and SDSS J1511+0607 are shown in Figure 9. The most likely semi-major axes are demarcated by a dashed red line and the central 68% ($\pm 1\sigma$ equivalent) of the data are shaded in lavender. We estimated the periods for these orbits in years assuming $P^2 = a^3/M_{tot}$, with $M_{tot} = M_1 + M_2$ in Solar masses estimated from the models of Baraffe et al. (2003) for ages of 0.5, 1, 5 and 10 Gyr (Table 7). For 2MASS J1341−3052, we obtain most likely semi-major axis and period of $8.6^{+5.2}_{-1.8}$ AU and 63−85 years for decreasing ages, while for SDSS J1511+0607 the most likely semi-major axis and periods are $3.4^{+1.8}_{-0.8}$ AU and 15−21 years.

4.3. On the frequency of short period VLM binaries

Starting from a sample of LGS-AO observations of 43 brown dwarfs, we resolved 3 of 17 spectral binary candidates and none of the other targets. 2MASS J1733−1654 has a particularly asymmetrical PSF shape which could indicate the presence of a marginally resolved companion NE of the primary, but this is inconclusive from our images. The fraction of resolved systems from the spectral binary sample is $3/17 = 18^{+13}_{-6}\%$ (binomial uncertainties), which is consistent with the observed binary fractions reported in the literature from imaging programs ($10 - 20\%$; Bouy et al. 2003; Close et al. 2003; Basri & Reiners 2006; Allen 2007; Burgasser 2007a; Kraus & Hillenbrand 2012). Among the spectral binaries, 2MASS J0518−2828, WISEP J0720−0846, SDSS J0805+4812, 2MASS J1106+2754 and 2MASS J1209−1004 are known binaries unresolved in our images. This indicates a minimum binary fraction for spectral binaries in this sample of $(3 + 5)/17 = 47^{+12}_{-11}\%$. This is considerably higher than typical VLM binary search samples and indicates that the spectral binary sample is positively biased towards binaries. The fact that over half of the known binaries in this sample are not resolved suggests that imaging programs are similarly missing binaries, and that the true binary fraction may be significantly higher than what is currently reported. Note that the fraction reported here remains a lower limit; an unknown number of the 9 unresolved and unconfirmed spectral binaries may be true binaries with separations $\lesssim 1.5 - 9.2$ AU.

Of the 12 confirmed spectral binaries to date (Table 8), about half have been unresolved in reported LGS-AO imaging, which is roughly consistent with the 3 resolved and 5 unresolved binaries in our sample. While follow-up of unresolved systems is more time-consuming and resource-intensive (radial velocity and astrometric monitoring), we speculate that the number of unresolved but confirmed spectral binaries will increase as follow-up is completed. A high incidence of unresolved but confirmed spectral binaries implies a high incidence of currently unresolved binaries in general. For example, if all of the unresolved spectral binaries in our sample actually are binaries, this would indicate a ratio of unresolved-to-resolved systems of 4.7:1. Given that the resolved binary fraction is roughly 15%, this rate of unresolved pairs would imply an overall binary fraction of over 60%. It is more likely that the current pool of spectral binary candidates contains some number of contaminants, such as blue L dwarfs (BG14) and variable brown dwarfs (Khandrika et al. 2013; Radigan et al. 2012) which will need to be identified through more detailed spectral and photometric variability analysis. Nevertheless, it is important to note that all 17 spectral binary systems studied here have resolved or upper limit separations near or below the peak of the resolved binary separation of VLM dwarfs (Allen 2007). This is strong evidence that a large number of VLM binaries are being missed in current imaging surveys.

5. Summary

We have observed 43 late-M, L and T dwarfs with Keck/NIRC2 LGS-AO, including 17 spectral binary candidates with high resolution Keck/NIRC2 LGS-AO imaging. Three sources were resolved: 2MASS J1341−3052, SDSS J1511+0607 and SDSS J2052−1609, while five other confirmed binaries were unresolved. Only one of our spectral binary candidates, 2MASS J1733−1654, has a candidate faint companion on the images, requiring confirmation. We used relative photometry to update the estimated component spectral types of our resolved systems. For SDSS J2052−1609, we combined our observations with those of Stumpf et al. (2011) and archival data to make a preliminary determination of orbital parameters, finding a period of 33^{+4}_{-2} years and system mass of $0.0823^{+0.0037}_{-0.0017} M_\odot$ consistent with a relatively young system (0.4−1.4 Gyr). For 2MASS J1341−3052 and SDSS J1511+0607, we estimated their most likely semi-major axes and periods

based on their observed angular separations, distances and estimated masses. 2MASS J1341−3052 has a projected separation of 8.1±0.5 AU and a period in the range of $63 - 85$ years depending on the ages. For SDSS J1511+0607, we estimate a projected separation of 2.9±0.3 AU and a period in the $17 - 25$ years range.

For the remaining 14 unresolved spectral binaries we calculated separation limits based on their estimated component magnitude differences from template fitting and empirical sensitivity curves. Five of these unresolved systems are confirmed binaries with measured angular separations smaller than our upper limits, and therefore consistent. The other 9 unresolved systems have upper limits in angular separation of $0\farcs04 - 0\farcs28$, corresponding to projected separations limits of $1.5 - 9.2$AU.

The binary fraction of the spectral binary candidates in this sample is $47^{+12}_{-11}\%$, significantly higher than those from prior imaging surveys (10−20%; Bouy et al. 2003; Burgasser et al. 2003; Cruz et al. 2003) and the overall binary fraction (20−25%; Basri & Reiners 2006; Burgasser 2007a; Joergens 2008). While this sample is clearly biased towards binary systems, the high percentage of unresolved systems suggests that there may exist a large population of very tight brown dwarf binaries that cannot be confirmed with high resolution imaging. Confirmation of the 9 remaining unresolved spectral binaries depends on high resolution radial velocity or astrometric variability measurements that are currently ongoing. If these unresolved sources turn out to be binaries, a great advantage of their short projected separation is the high likelihood for full orbit and dynamical mass determinations. In any case, an unbiased, volume-limited sample of spectral binaries with complete follow-up is required in order to find the true underlying binary fraction.

Acknowledgements

We would like to thank our referee Sandy Leggett for her helpful comments. The authors thank observing assistants Jason McIlroy, Heather Hershley, Terry Stickel, and Gary Puniwai and support astronomers Hien Tran, Luca Rizzi, Marc Kassis, and Al Conrad for their assistance during our observations. DBG acknowledges funding support from the IPAC graduate fellowship. DBG and AJB acknowledge support from the National Aeronautics and Space Administration under Grant No. NNX15AI75G. CRG was partially supported by a NASA Keck PI Data Award, administered by the NASA Exoplanet Science Institute. This research has made use of the Keck Observatory Archive (KOA), which is operated by the W. M. Keck Observatory and the NASA Exoplanet Science Institute (NExScI), under contract with the National Aeronautics and Space Administration. This publication makes use of data from the SpeX Prism Spectral Libraries, maintained by Adam Burgasser at `http://www.browndwarfs.org/spexprism`; the Dwarf Archives Compendium, maintained by Chris Gelino, Davy Kirkpatrick, Mike Cushing, David Kinder and Adam Burgasser at `http://DwarfArchives.org`; and the VLM Binaries Archive maintained by Nick Siegler at `http://vlmbinaries.org`. The authors wish to recognize and acknowledge the very significant cultural role and reverence that the summit of Mauna Kea has always had within the indigenous Hawaiian community. We are most fortunate to have the opportunity to conduct observations from this mountain.

Facilities: Keck NIRC2.

REFERENCES

Adelman-McCarthy, J. K., Agüeros, M. A., Allam, S. S., et al. 2007, ApJS, 172, 634, 634

Allen, P. R. 2007, ApJ, 668, 492, 492

Baraffe, I., Chabrier, G., Barman, T. S., Allard, F., & Hauschildt, P. H. 2003, A&A, 402, 701, 701

Bardalez Gagliuffi, D. C., Burgasser, A. J., Gelino, C. R., et al. 2014, ApJ, 794, 143, 143

Basri, G., & Reiners, A. 2006, AJ, 132, 663, 663

Blake, C. H., Charbonneau, D., White, R. J., et al. 2008, ApJ, 678, L125, L125

Bouy, H., Brandner, W., Martín, E. L., et al. 2003, AJ, 126, 1526, 1526

Burgasser, A. J. 2007a, ApJ, 659, 655, 655

—. 2007b, AJ, 134, 1330, 1330

Burgasser, A. J. 2014, in Astronomical Society of India Conference Series, Vol. 11, Astronomical Society of India Conference Series, 7–16

Burgasser, A. J., Bardalez-Gagliuffi, D. C., & Gizis, J. E. 2011a, AJ, 141, 70, 70

Burgasser, A. J., Burrows, A., & Kirkpatrick, J. D. 2006a, ApJ, 639, 1095, 1095

Burgasser, A. J., Cruz, K. L., Cushing, M., et al. 2010, ApJ, 710, 1142, 1142

Burgasser, A. J., Kirkpatrick, J. D., Cruz, K. L., et al. 2006b, ApJS, 166, 585, 585

Burgasser, A. J., Kirkpatrick, J. D., Reid, I. N., et al. 2003, ApJ, 586, 512, 512

Burgasser, A. J., Liu, M. C., Ireland, M. J., Cruz, K. L., & Dupuy, T. J. 2008, ApJ, 681, 579, 579

Burgasser, A. J., Luk, C., Dhital, S., et al. 2012, ApJ, 757, 110, 110

Burgasser, A. J., McElwain, M. W., Kirkpatrick, J. D., et al. 2004, AJ, 127, 2856, 2856

Burgasser, A. J., Melis, C., Todd, J., et al. 2015a, ArXiv e-prints, arXiv:1508.06332

Burgasser, A. J., Reid, I. N., Siegler, N., et al. 2007, Protostars and Planets V, 427, 427

Burgasser, A. J., Sitarski, B. N., Gelino, C. R., Logsdon, S. E., & Perrin, M. D. 2011b, ApJ, 739, 49, 49

Burgasser, A. J., Gillon, M., Melis, C., et al. 2015b, AJ, 149, 104, 104

Carson, J. C., Marengo, M., Patten, B. M., et al. 2011, ApJ, 743, 141, 141

Chiu, K., Fan, X., Leggett, S. K., et al. 2006, AJ, 131, 2722, 2722

Close, L. M., Siegler, N., Freed, M., & Biller, B. 2003, ApJ, 587, 407, 407

Cruz, K. L., Burgasser, A. J., Reid, I. N., & Liebert, J. 2004, ApJ, 604, L61, L61

Cruz, K. L., Reid, I. N., Liebert, J., Kirkpatrick, J. D., & Lowrance, P. J. 2003, AJ, 126, 2421, 2421

Cutri, R. M., Skrutskie, M. F., van Dyk, S., et al. 2003, VizieR Online Data Catalog, 2246, 0, 0

Day-Jones, A. C., Marocco, F., Pinfield, D. J., et al. 2013, MNRAS, 648, 648

Dupuy, T. J., & Liu, M. C. 2011, ApJ, 733, 122, 122

—. 2012, ApJS, 201, 19, 19

Dupuy, T. J., Liu, M. C., & Ireland, M. J. 2014, ApJ, 790, 133, 133

Duquennoy, A., & Mayor, M. 1991, A&A, 248, 485, 485

Faherty, J. K., Burgasser, A. J., Cruz, K. L., et al. 2009, AJ, 137, 1, 1

Faherty, J. K., Burgasser, A. J., Walter, F. M., et al. 2012, ApJ, 752, 56, 56

Fischer, D. A., & Marcy, G. W. 1992, ApJ, 396, 178, 178

Geißler, K., Metchev, S., Kirkpatrick, J. D., Berriman, G. B., & Looper, D. 2011, ApJ, 732, 56, 56

Gelino, C. R., & Burgasser, A. J. 2010, AJ, 140, 110, 110

Hastings, W. K. 1970, Biometrika, 57, 97, 97

Hawley, S. L., Covey, K. R., Knapp, G. R., et al. 2002, AJ, 123, 3409, 3409

Innes, R. T. A. 1907, The Observatory, 30, 310, 310

Joergens, V. 2008, A&A, 492, 545, 545

Khandrika, H., Burgasser, A. J., Melis, C., et al. 2013, AJ, 145, 71, 71

Kirkpatrick, J. D., Looper, D. L., Burgasser, A. J., et al. 2010, ApJS, 190, 100, 100

Konopacky, Q. M., Ghez, A. M., Barman, T. S., et al. 2010, ApJ, 711, 1087, 1087

Kraus, A. L., & Hillenbrand, L. A. 2012, ApJ, 757, 141, 141

Liu, M. C., Dupuy, T. J., & Leggett, S. K. 2010, ApJ, 722, 311, 311

Looper, D. L., Gelino, C. R., Burgasser, A. J., & Kirkpatrick, J. D. 2008a, ApJ, 685, 1183, 1183

Looper, D. L., Kirkpatrick, J. D., & Burgasser, A. J. 2007, AJ, 134, 1162, 1162

Looper, D. L., Kirkpatrick, J. D., Cutri, R. M., et al. 2008b, ApJ, 686, 528, 528

Manjavacas, E., Goldman, B., Reffert, S., & Henning, T. 2013, A&A, 560, A52, A52

Metchev, S. A., Kirkpatrick, J. D., Berriman, G. B., & Looper, D. 2008, ApJ, 676, 1281, 1281

Metropolis, N., Rosenbluth, A. W., Rosenbluth, M. N., Teller, A. H., & Teller, E. 1953, J. Chem. Phys., 21, 1087, 1087

Monet, D. G., Levine, S. E., Canzian, B., et al. 2003, AJ, 125, 984, 984

Pravdo, S. H., Shaklan, S. B., Wiktorowicz, S. J., et al. 2006, ApJ, 649, 389, 389

Radigan, J., Jayawardhana, R., Lafrenière, D., et al. 2012, ApJ, 750, 105, 105

Raghavan, D., McAlister, H. A., Henry, T. J., et al. 2010, ApJS, 190, 1, 1

Rayner, J. T., Toomey, D. W., Onaka, P. M., et al. 2003, PASP, 115, 362, 362

Reid, I. N., Cruz, K. L., Kirkpatrick, J. D., et al. 2008, AJ, 136, 1290, 1290

Saumon, D., & Marley, M. S. 2008, ApJ, 689, 1327, 1327

Scholz, R.-D. 2014, A&A, 561, A113, A113

Silvestri, N. M., Lemagie, M. P., Hawley, S. L., et al. 2007, AJ, 134, 741, 741

Simons, D. A., & Tokunaga, A. 2002, PASP, 114, 169, 169

Stephens, D. C., Leggett, S. K., Cushing, M. C., et al. 2009, ApJ, 702, 154, 154

Stumpf, M. B., Geißler, K., Bouy, H., et al. 2011, A&A, 525, A123, A123

Tokunaga, A. T., Simons, D. A., & Vacca, W. D. 2002, PASP, 114, 180, 180

van Dam, M. A., Bouchez, A. H., Le Mignant, D., et al. 2006, PASP, 118, 310, 310

van den Bos, W. H. 1927, Bull. Astron. Inst. Netherlands, 3, 261, 261

Wizinowich, P. L., Le Mignant, D., Bouchez, A. H., et al. 2006, PASP, 118, 297, 297

This preprint was prepared with the AAS LaTeX macros v5.2.

Table 1. Observation Log

Name	SpT	2MASS H	Date	Reference Star	Filter	t_{exp}(s)	Airmass	Strehl Ratio	S/N
Spectral Binaries from B10 and BG14									
SDSS J011912.22+240331.6	T2	16.46 ± 0.03	2009 Aug 15	1140-0016097	H	720	1.02	0.25	717
			2013 Sep 22	1140-0016097	H	120	1.01	0.01	103
			2013 Sep 23	1140-0016097	H	120	1.05	0.23	897
SDSS J024749.90−163112.6	T2	16.31 ± 0.03	2009 Aug 15	0734-0037544	H	720	1.32	0.11	764
2MASS J03440892+0111251	L0.5	13.91 ± 0.04	2013 Sep 22	0911-0037820	H	175	1.07	0.15	3043
SDSS J035104.37+481046.8	T1	15.57 ± 0.14	2009 Aug 15	1381-0118655	H	720	1.38	0.14	894
2MASS J05185995−2828372	T1	14.83 ± 0.07	2013 Sep 23	0615-0055796	H	120	1.63	0.12	1718
WISE J07200320−0846513	M9.5	9.92 ± 0.02	2014 Jan 19	0812-0137371	H	60	1.28	0.02	1638
SDSS J080531.84+481233.0	L9	13.92 ± 0.04	2010 Mar 24	1382-0223846	K_s	540	1.21	0.12	2624
			2013 Sep 23	1382-0223846	H	120	1.61	0.09	3029
2MASS J11061197+2754225	T2.5	14.15 ± 0.05	2010 Mar 24	1179-0233699	H	720	1.03	0.07	2559
2MASS J12095613−1004008	T3	15.33 ± 0.09	2014 Jan 13	0799-0230529	H	120	1.15	0.04	1146
2MASS J13411160−3052505	L3	13.72 ± 0.03	2014 Jan 13	0591-0304901	J	120	1.61	0.02	807
			2014 Jan 13	0591-0304901	H	120	1.65	0.04	1508
			2014 Jan 19	0591-0304901	H	120	1.59	0.04	1845
			2014 Jan 13	0591-0304901	K_s	180	1.59	0.05	1861
SDSS J143553.25+112948.6	T2	16.52 ± 0.04	2009 Aug 15	1014-0229971	H	360	1.25	0.05	373
			2009 Aug 15	1014-0229971	K_s	360	1.30	0.08	268
SDSS J151114.66+060742.9	T0	14.96 ± 0.08	2009 Aug 15	0961-0243717	J	360	1.36	0.01	560
			2009 Aug 15	0961-0243717	H	360	1.27	0.09	1078
			2009 Aug 15	0961-0243717	K_s	720	1.32	0.13	1101
			2010 May 19	0961-0243717	H	120	1.03	0.09	94
SDSS J151643.01+305344.4	T0.5	15.87 ± 0.16	2010 Mar 24	0930-0297471	H	720	1.04	0.06	1007
SDSS J154727.23+033636.3	L2	15.07 ± 0.06	2009 Aug 15	0936-0258682	H	720	1.40	0.01	805
2MASS J1711457+223204	L6.5	15.80 ± 0.11	2010 May 13	1125-0317350	J	720	1.22	0.05	381
			2010 May 13	1125-0317350	H	720	1.27	0.07	844
2MASS J1733423−165449	L0.5	12.81 ± 0.06	2009 Aug 15	0730-0518366	J	720	1.39	0.08	2324
			2009 Aug 15	0730-0518366	H	720	1.36	0.10	2748
SDSS J205235.31−160929.8	T1	15.45 ± 0.03	2009 Aug 15	0738-0802833	J	360	1.30	0.06	543
			2009 Aug 15	0738-0802833	H	360	1.27	0.00	1003
			2009 Aug 15	0738-0802833	K_s	360	1.28	0.17	729
Visually Selected Spectral Binary Candidates									

Table 1—Continued

Name	SpT	2MASS H	Date	Reference Star	Filter	t_{exp}(s)	Airmass	Strehl Ratio	S/N
2MASS J0019457+521317	M9	12.07 ± 0.02	2009 Aug 15	1422-0011510	J	360	1.30	0.09	2502
			2009 Aug 15	1422-0011510	H	720	1.28	0.25	5028
2MASS J00320509+0219017	L1.5	13.39 ± 0.02	2009 Aug 15	0923-0006944	H	720	1.10	0.11	2811
SDSS J003259.36+141036.6	L8	15.65 ± 0.14	2009 Aug 15	1041-0005438	H	720	1.02	0.10	1112
			2009 Aug 15	1041-0005438	K_s	360	1.02	0.11	721
2MASS J02361794+0048548	L6.5	15.27 ± 0.07	2013 Sep 22	0908-0027044	H	180	1.06	0.14	1959
SDSS J075840.33+324723.4	T2	14.11 ± 0.04	2010 Mar 24	1227-0198441	H	720	1.06	0.05	2333
SDSS J093109.56+032732.5	L7.5	16.27 ± 0.24	2010 Mar 24	0934-0195871	H	720	1.18	0.03	611
2MASS J09490860−1545485	T2	15.26 ± 0.11	2010 Mar 24	0742-0216967	H	720	1.24	0.05	1399
SDSS J103321.92+400549.5	L6	16.05 ± 0.04	2010 Mar 24	1300-0206652	H	720	1.07	0.06	828
SDSS J112118.57+433246.5	L7.5	16.56 ± 0.04	2010 Mar 24	3015-00408-1	H	720	1.16	0.08	674
2MASS J11582073+0435022	sdL7	14.68 ± 0.06	2010 May 13	0945-0201532	H	720	1.04	0.15	1776
			2010 May 13	0945-0201532	K_s	720	1.04	0.23	1882
SDSS J120602.51+281328.7	T3	15.83 ± 0.03	2010 Mar 24	1182-0220446	H	720	1.11	0.10	197
2MASS J14283132+5923354	L4	13.88 ± 0.04	2010 May 19	1493-0219430	H	720	1.29	0.10	3219
2MASS J1707333+430130	L0.5	13.18 ± 0.03	2009 Aug 15	1330-0334426	H	720	1.41	0.08	2425
2MASS J1721039+334415	L3	12.95 ± 0.03	2009 Aug 15	1237-0272128	H	720	1.21	0.11	953
			2010 Mar 24	1237-0272128	H	720	1.03	0.07	2721
2MASS J21265916+7617440	T0	13.59 ± 0.04	2013 Sep 23	1662-0097897	H	120	2.16	0.08	79
SDSS J214956.55+060334	M9	12.63 ± 0.03	2009 Aug 15	0960-0568745	H	720	1.08	0.09	2670
Additional Targets									
WISEP J004701.06+680352.1	L7.5	13.97 ± 0.04	2013 Sep 23	1580-0021858	H	90	1.56	0.28	2410
2MASS J03001631+2130205	L6p	14.73 ± 0.07	2013 Sep 22	1115-0038422	H	120	1.06	0.13	1583
2MASS J03020122+1358142	L3	15.43 ± 0.09	2013 Sep 23	1039-0030470	H	120	1.01	0.05	944
HYT0429+1535	···	···	2013 Sep 22	1031-0059287	CH_4	120	1.01	0.16	131
			2013 Sep 22	1031-0059287	H	120	1.00	0.17	88
2MASSI J0443058−320209	L5	14.35 ± 0.06	2013 Sep 22	0579-0075735	H	120	1.67	0.07	2206
WISE J052857.69+090104.4	M9.5p	15.44 ± 0.12	2014 Jan 19	0990-0058827	H	135	1.40	0.07	99
SDSS J115013.17+052012.3	L6	15.46 ± 0.14	2014 Jan 13	0279-01016-1	H	60	1.03	0.17	993
ULAS J132605.18+120009.9	T6p	17.93 ± 0.09	2010 May 19	1019-0249297	H	720	1.02	0.24	371
2MASS J14140586+0107102	L4.8:	15.73 ± 0.19	2010 May 13	0317-00292-1	H	720	1.07	0.20	1168
2MASS J20025073−0521524	L6	14.28 ± 0.05	2009 Aug 15	0846-0581639	H	360	1.35	0.12	1709

Table 2. Updated index selection criteria for B10 and BG14.

x	y	Limits
		Burgasser et al. (2010)
H_2O-J	H_2O-K	$0.325 < x < 0.65$ and $y > 0.615x + 0.300$
CH_4-H	CH_4-K	$0.6 < x < 1.0$ and $y > 1.063x - 0.288$
CH_4-H	K/J	$0.65 < x < 1.00$ and $y > 0.471x - 0.096$
H_2O-H	H-dip	$0.44 < x < 0.68$ and $y < 0.49$
SpT	H_2O-J/H_2O-H	L8.5< x <T3.5, $y < 0.925$ and $y < -0.037x + 2.106$
SpT	H_2O-J/CH_4-K	L8< x <T4.5 and $y < 0.041x - 0.517$
		Bardalez Gagliuffi et al. (2014)
SpT	CH_4-H	$M7.5 < x < L8$ and $y < -4.3 \times 10^{-4}x^2 + 0.0253x + 0.6824$
H_2O-J	CH_4-H	$0.60 < x < 0.92$ and $y < -0.094x + 1.096$.
H_2O-J	H-bump	$0.65 < x < 0.90$ and $y > 0.16x + 0.806$.
CH_4-J	CH_4-H	$0.6 < x < 1.04$, $y < 1.04$ and $y < -0.562x + 1.417$.
CH_4-J	H-bump	$0.60 < x < 0.74$, $y > 0.91$ and $y > 1.00x + 0.24$.
CH_4-H	J-slope	$0.94 < x < 1.03$, $y > 1.03$ and $y > 1.250x - 0.207$.
CH_4-H	J-curve	$0.95 < x < 1.03$ and $y > 1.245x^2 - 1.565x + 2.312$.
CH_4-H	H-bump	$0.94 < x < 1.04$, $y > 0.92$ and $y < 1.36x^2 - 4.26x + 3.877$.
J-slope	H-dip	$1.03 < x < 1.13$ and $y < 0.20x + 0.27$.
J-slope	H-bump	$1.025 < x < 1.130$, $y > -2.75x + 3.84$ and $y > 0.91$.
K-slope	H_2O-Y	$0.93 < x < 0.96$ and $y > 12.036x^2 - 20.000x + 9.037$.
J-curve	H-bump	$2.00 < x < 2.45$, $y > 0.92$ and $y > 0.269x^2 - 1.326x + 2.527$.

Table 3. Projected separation constraints for spectral binaries and all other targets.

Source	Spectral Type			2MASS ΔJ	2MASS ΔH	2MASS ΔK	Confidence	Distance (pc)	Ref.	Separation	
	Optical*	Primary	Secondary							Angular (mas)	Projected (AU)
Spectral Binaries											
SDSS J011912.22+240331.6	T2.0	T0.3±0.7	T3.7±0.5	-0.28±0.13	0.30±0.11	0.82±0.20	> 99%	43±3	1	< 43	< 1.9
SDSS J024749.90−163112.6	T2.0	L8.4±0.6	T5.7±0.5	0.57±0.30	1.62±0.33	2.10±0.30	100%	40±3	1	< 96	< 3.8
2MASS J03440892+0111251	L0.5	L0.3±0.4	T3.8±1.5	2.77±0.38	3.10±0.65	3.50±0.70	98%	41±4	1	< 226	< 9.2
SDSS J035104.37+481046.8	T1.0	L6.3±0.7	T5.4±0.9	0.45±0.47	1.62±0.51	2.45±0.52	> 99%	37±4	1	< 102	<3.8
2MASS J05185995−2828372	···	L6.4±0.4	T5.6±0.5	0.54±0.25	1.75±0.27	2.48±0.28	100%	$23\pm1^{\pi}$	4	< 98	< 2.2
WISE J07200320−0846513	···	M8.9±0.0	T5.2±0.7	3.50±0.24	4.15±0.36	4.57±0.41	100%	$6\pm1^{\pi}$	2	< 500	< 3.0
SDSS J080531.84+481233.0	L9.0	L5.3±0.1	T5.8±0.4	1.92±0.17	2.85±0.18	3.49±0.30	100%	$23\pm1^{\pi}$	4	< 164	< 3.8
2MASS J11061197+2754225	T2.5	L8.9±0.5	T4.2±0.4	-0.24±0.14	0.49±0.17	1.03±0.16	100%	$21\pm1^{\pi}$	3	< 74	< 1.5
2MASS J12095613−1004008	···	T1.1±0.0	T6.0±0.4	0.95±0.11	1.77±0.15	2.10±0.28	> 99%	$22\pm1^{\pi}$	4	< 100	< 2.1
2MASS J13411160−30525049†	L3.0	L2.3±0.6	T6.0±1.0	2.68±0.08	4.03±0.12	4.23±0.07	96%	29±3	1	279±17	8.9 ± 0.4
SDSS J143553.25+112948.6	T2.0	L8.9±0.7	T5.6±0.5	0.28±0.24	1.38±0.28	2.11±0.37	> 99%	44±4	1	< 90	< 4.0
SDSS J151114.66+060742.9†	T0.0	L5.2±0.9	T4.9±0.4	0.25±0.13	1.41±0.13	2.38±0.30	> 99%	$28\pm5^{\pi}$	5	108±11	2.9±0.3
SDSS J151643.01+305344.4	T0.5	L7.6±0.8	T2.3±0.3	-0.36±0.24	0.21±0.21	0.80±0.27	99%	39±4	1	< 70	< 2.7
SDSS J154727.23+033636.3	L2.0	L1.8±0.2	T6.6±1.0	3.32±0.53	4.38±0.60	4.98±0.65	90%	53±6	1	Unconstrained	Unconstrained
2MASS J1711457+223204	L6.5	L5.5±0.5	T5.3±1.0	1.21±0.41	2.29±0.56	3.08±0.64	> 99%	$30\pm4^{\pi}$	4	< 156	< 4.7
2MASS J1733423−165449	L0.5	L0.1±0.2	T4.0±1.3	2.76±0.30	3.14±0.54	3.59±0.60	98%	24±2	1	< 219	< 5.3
SDSS J205235.31−160929.8†	T1.0	L5.9±1.6	T2.1±0.5	0.03±0.25	0.44±0.30	1.12±0.40	> 99%	$30\pm1^{\pi}$	4	103±2	3.2±0.5
Visual Spectral Binaries											
2MASSI J0019457+521317	M9.0	M8.5±0.2	T6.9±1.1	4.82±0.54	5.53±0.65	5.91±0.71	50%	20±2	1	Unconstrained	Unconstrained
2MASS J00320509+0219017	L1.5	L0.1±0.3	T6.4±1.4	4.06±0.68	4.87±0.83	5.36±0.85	49%	33±4	1	Unconstrained	Unconstrained
SDSS J003259.36+141036.6	L8.0	L6.2±0.7	T2.4±1.9	0.55±0.70	1.03±0.95	1.54±0.97	50%	$33\pm6^{\pi}$	4	< 96	< 3.2
SDSSp J023617.93+004855.0	L6.5	L5.1±0.5	T1.9±1.2	1.04±0.49	1.33±0.59	1.81±0.58	7%	39±4	1	< 95	< 3.7
SDSS J075840.33+324723.4	T2.0	T2.3±0.0	T2.2±0.0	-0.28±0.0	-0.07±0.0	0.193±0.0	92%	16±2	1	< 65	< 1.0
SDSS J093109.56+032732.5	L7.5	L7.2±0.3	T6.6±1.8	2.66±0.49	3.45±0.78	3.87±0.91	90%	37±4	1	< 288	< 10.7
2MASS J09490860−1545485	T2.0	T1.1±0.2	T3.5±2.0	0.54±1.01	0.83±1.28	0.83±1.26	95%	$18\pm2^{\pi}$	5	< 101	< 1.8
SDSS J103321.92+400549.5	L6.0	L4.9±0.6	T4.4±2.2	1.96±0.72	2.52±1.02	2.99±1.07	84%	54±6	1	< 206	< 11.2
SDSS J112118.57+433246.5	L7.5	L6.8±0.5	T5.0±1.5	1.52±0.64	2.21±0.80	2.74±0.84	95%	52±6	1	< 164	< 8.4
2MASS J11582077+0435014	sdL7	L6.4±0.0	T2.6±0.8	1.42±0.12	1.57±0.22	1.98±0.26	100%	28±2	1	< 93	< 2.5
SDSS J120602.51+281328.7	T3.0	T2.0±0.4	T5.0±0.8	0.46±0.35	1.05±0.49	1.26±0.50	74%	29±3	1	< 87	< 2.5
2MASS J14283132+5923354	L4.0	L4.4±0.7	T6.4±2.0	3.30±0.72	4.24±1.00	4.77±1.06	68%	21±3	1	Unconstrained	Unconstrained
2MASS J17073334+4301304	L0.5	M8.7±0.1	T6.9±0.7	4.41±0.47	5.28±0.51	5.75±0.53	60%	35±3	1	Unconstrained	Unconstrained
2MASS J1721039+334415	L3.0	L2.5±0.0	T3.8±2.0	2.91±0.62	3.10±0.99	3.32±1.09	99%	19±2	1	< 270	< 5.1
2MASS J21265916+7617440	T0.0	L8.5±1.0	T4.5±2.0	0.42±0.82	1.21±1.01	1.75±1.03	63%	12±2	1	< 106	< 1.3
SDSS J214956.55+060334	M9.0	M8.2±0.0	T6.6±1.2	4.83±0.59	5.53±0.70	5.91±0.74	58%	29±3	1	Unconstrained	Unconstrained

*Unresolved or combined optical spectral type.

†Resolved binary with *measured* delta magnitudes.

[π] Parallactic distance. Otherwise, spectrophotometric distance, assuming relative magnitudes from template fitting.

References. — (1) This paper; (2) Burgasser et al. (2015b); (3) Manjavacas et al. (2013); (4) Dupuy & Liu (2012); (5) Faherty et al. (2012).

Table 4. Properties of three resolved binary systems.

Parameter	2MASS J1341−3052	SDSS J1511+0607	SDSS J2052−1609
Primary SpT	L2.5±1.0	L5.5±1.0	L6.0±2.0
Secondary SpT	T6.0±1.0	T5.0±0.5	T2.0±0.5
ΔJ	2.68±0.08	0.25±0.13	0.03±0.25
ΔH	4.03±0.12	1.41±0.13	0.44±0.30
ΔK_s	4.23±0.07	2.38±0.30	1.12±0.40
Distance (pc)	29±3[1]	28±5[2]	30±1[3]
Ang. Sep. (*mas*)	279±17	108±11	103±2
Proj. Sep. (AU)	8.1±0.5	2.9±0.3	3.0±0.1
PA (°)	317.9±0.6	335.0±4.3	68.4±1.1
Epoch (JD)	2456671.15	2455058.77	2455058.94

[1]This paper.

[2]Faherty et al. (2012)

[3]Dupuy & Liu (2012)

Table 5. Resolved Separation Measurements for SDSS J2052−1609AB

UT Date	JD	Instrument	$\Delta\alpha$ (mas)	$\Delta\delta$ (mas)	Ref
2005 Oct 11	2453654	Keck/NIRC2	25.4±1.2	114.3±1.4	1,2
2007 Apr 23	2454213	Keck/NIRC2	54.6±2.1	88.8±1.5	1,2
2008 Jun 24	2454642	HST/NICMOS	79.2±0.9	65.6±0.8	3
2009 Jun 19	2455002	VLT/NACO	93.1±1.0	38.9±0.9	3
2009 Aug 15	2455058	Keck/NIRC2	95.7±0.7	38.1±0.7	1
2010 May 01	2455317	Keck/NIRC2	103.4±1.7	20.6±1.5	1,4

References. — (1) This paper; (2) NIRC2 PI M. Liu; (3) Stumpf et al. (2011); (4) NIRC2 PI B. Biller.

Table 6. Orbital Analysis of SDSS J2052−1609AB Relative Astrometry

Parameter	Best	Median
Best χ^2 (DOF)	12.05 (6)	···
P^{a} (yr)	32	33^{+4}_{-2}
a (AU)	4.4	$4.5^{+0.5}_{-0.2}$
e^{a}	0.005	$0.014^{+0.023}_{-0.010}$
i (°)	45	45^{+5}_{-3}
ω (°)	98	100^{+15}_{-13}
Ω (°)	327	327^{+3}_{-4}
M_0 (°)	318	313^{+15}_{-8}
d^{a} (pc)	30.5	$30.7^{+0.2}_{-0.4}$
M_{tot} ($M_\odot$)	0.081	$0.0823^{+0.0037}_{-0.0017}$

[a]Parameter was constrained to a limited value range in MCMC analysis.

Table 7. Estimated masses and orbit results from Monte Carlo simulation.

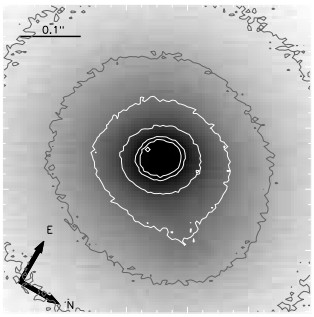
System	Age (Gyr)	Primary Mass ($M_\odot$)	Secondary Mass ($M_\odot$)	Semi-major Axis (AU)	Period (years)
2MASS J1341−3052AB	0.5	0.052±0.005	0.022±0.005	$8.6^{+5.2}_{-1.8}$	85^{+104}_{-20}
SpT = L2.5±1.0 and T6.0±1.0	1.0	0.065±0.004	0.030±0.007	$8.6^{+5.3}_{-1.8}$	71^{+91}_{-18}
Primary T_{eff} = 1904±165K	5.0	0.075±0.002	0.054±0.007	$8.6^{+5.3}_{-1.8}$	64^{+79}_{-15}
Secondary T_{eff} =1027±144K	10	0.075±0.001	0.061±0.006	$8.6^{+5.2}_{-1.8}$	63^{+76}_{-14}
SDSS J1511+0607AB	0.5	0.041±0.004	0.026±0.003	$3.4^{+1.8}_{-0.8}$	21^{+25}_{-5}
SpT = L5.0±1.0 and T5.0±0.5	1.0	0.052±0.005	0.035±0.004	$3.4^{+1.8}_{-0.9}$	18^{+22}_{-5}
Primary T_{eff} = 1617±139K	5.0	0.070±0.002	0.059±0.004	$3.4^{+1.7}_{-0.9}$	15^{+18}_{-3}
Secondary T_{eff} = 1115±107K	10	0.072±0.001	0.065±0.003	$3.4^{+1.8}_{-0.9}$	15^{+17}_{-4}

Table 8. Confirmed Spectral Binaries

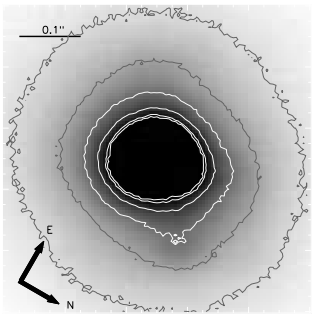
Name	Spectral Type				2MASS-J	$J-K_s$	ΔJ	Separations (AU)	Confirmation method*	Ref. SB;Conf.
	Combined Optical	Combined NIR	Primary	Secondary						
SDSS J000649.16−085246.3	M9	···	M8.5±0.5	T5±1	14.14±0.04	1.01±0.05	3.15±0.31	0.29±0.01	RV	5; 5
2MASS J03202839−0446358	M8:	L1	M8.5±0.3	T5±0.9	12.13±0.03	1.13±0.04	3.50±0.20	0.404±0.042	RV	8; 3
2MASS J05185995−2828372	···	···	L8.6±0.3	T6.4±1.0	15.98±0.10	1.82±0.12	0.13±0.19	1.8±0.5	DI	12; 10
WISEP J072003.20−084651.2	M9.5	···	M8.9±0.0	T5.2±0.7	10.63±0.02	1.16±0.03	3.30±0.20	0.84±0.17	DI	4; 4
SDSS J080531.84+481233.0	L4	L9.5	L5.1±0.4	T5.7±0.5	14.73±0.04	1.46±0.05	1.50±0.09	0.9-2.3	AV	9; 13
SDSS J092615.38+584720.9	T4.5	···	T4.0±0.1	T5.3±0.7	16.77±0.14	< 1.57	0.40±0.20	2.6±0.5	DI	16; 10, 11
2MASS J11061197+2754225	···	T2.5	T0.4±0.3	T4.0±0.8	14.82±0.04	1.02±0.07	-0.37±0.06	<2.67	OL	7, 14; 15
2MASS J12095613−1004008	···	T3	T1.2±0.3	T5.9±0.6	15.91±0.08	0.85±0.16	1.50±0.20	4.8±0.2	DI	1; 18
2MASS J13153094−2649513	L5	···	L4.9±0.5	T6.1±2.1	15.07±0.05	1.63±0.07	3.03±0.03	6.6±0.9	DI	6; 6
2MASS J13411160−30525049	L3	···	L2.3±0.6	T6.0±1.0	14.61±0.03	1.53±0.04	3.28±0.53	7.8±0.5	DI	2; 1
SDSS J151114.66+060742.9	···	T0±2	L5.2±0.9	T4.9±0.5	16.02±0.08	1.47±0.13	0.54±0.32	2.9±0.3	DI	7; 1
SDSS J205235.31−160929.8	···	T1±1	L5.8±1.8	T2.1±0.5	16.33±0.12	1.21±0.19	0.04±0.18	3.0±0.1	DI	7; 17

*RV = Radial velocity variability, DI = Direct imaging, AV = Astrometric variability, OL = Overluminosity.

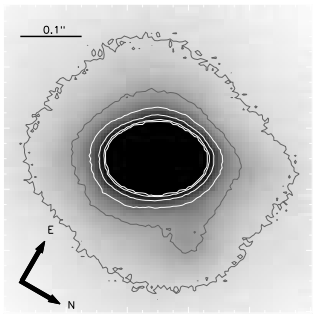
References. — (1) This paper; (2) Bardalez Gagliuffi et al. (2014); (3) Blake et al. (2008); (4) Burgasser et al. (2015b); (5) Burgasser et al. (2012); (6) Burgasser et al. (2011b); (7) Burgasser et al. (2010); (8) Burgasser et al. (2008); (9) Burgasser (2007b); (10) Burgasser et al. (2006b); (11) Carson et al. (2011); (12) Cruz et al. (2004); (13) Dupuy & Liu (2012); (14) Looper et al. (2008a); (15) Manjavacas et al. (2013); (16) Metchev et al. (2008); (17) Stumpf et al. (2011); (18) Liu et al. (2010).



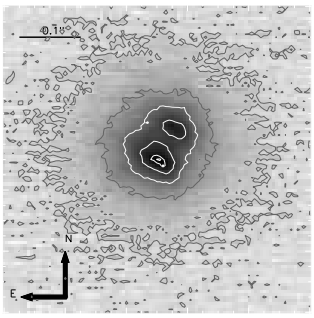
(a) *2MASS J1341-3052 J.*



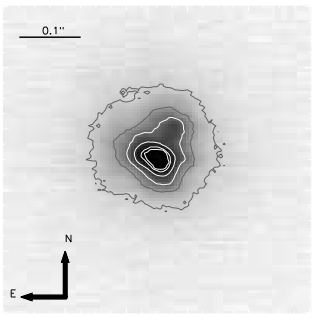
(b) *2MASS J1341-3052 H.*



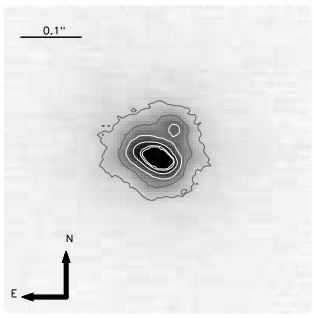
(c) *2MASS J1341-3052 K_s.*



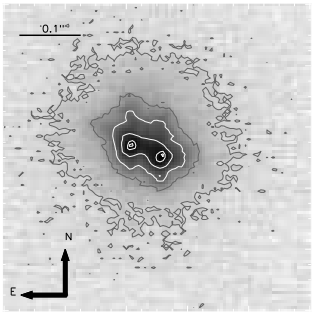
(d) *SDSS J1511+0607 J.*



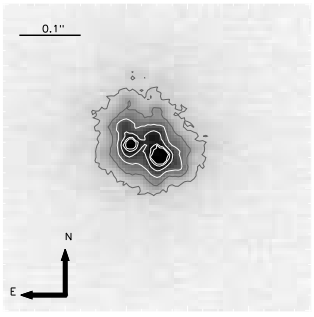
(e) *SDSS J1511+0607 H.*



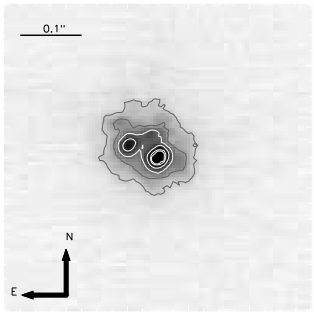
(f) *SDSS J1511+0607 K_s.*



(g) *SDSS J2052-1609 J.*

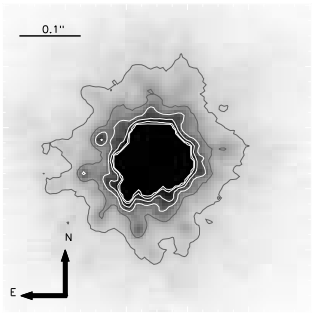


(h) *SDSS J2052-1609 H.*

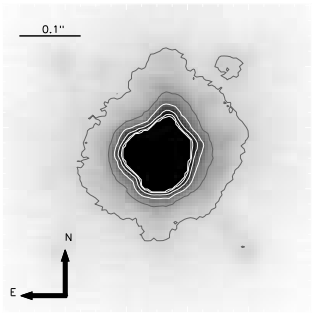


(i) *SDSS J2052-1609 K_s.*

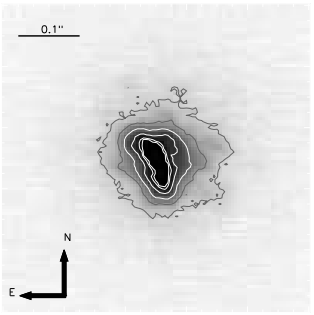
Fig. 1.— Keck NIRC2 LGS-AO images of the three binaries resolved in this sample in JHK_s bands.



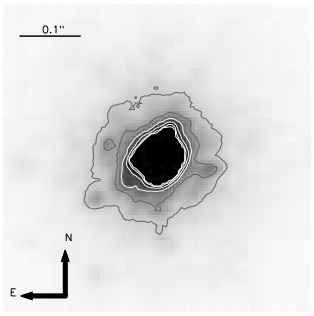
(i) *2MASSI J0019+5213*.



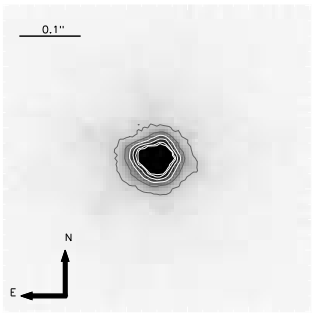
(ii) *2MASS J0032+0219*.



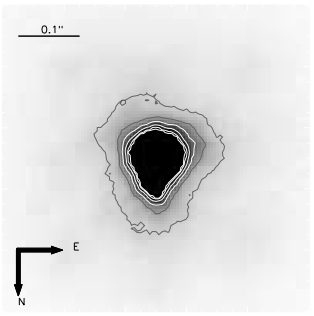
(iii) *SDSS J0032+1410*.



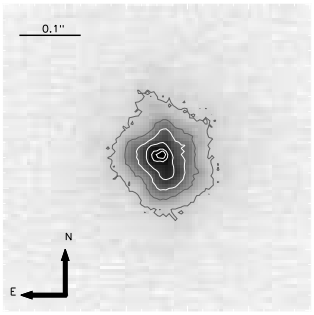
(iv) *WISEP J0047+6803*.



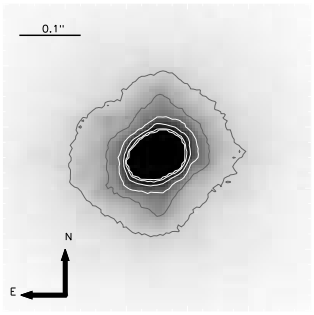
(v) *SDSS J0119+2403*.



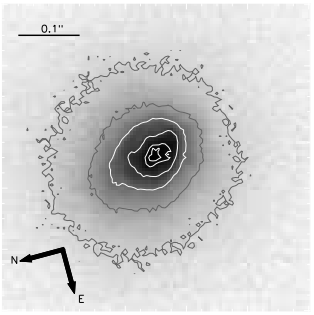
(vi) *SDSSp J0236+0048*.



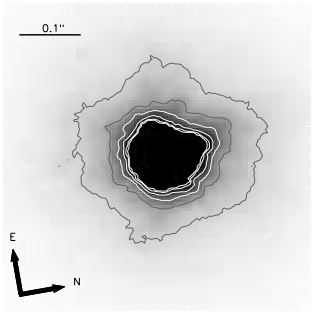
(vii) *SDSS J0247-1631*.



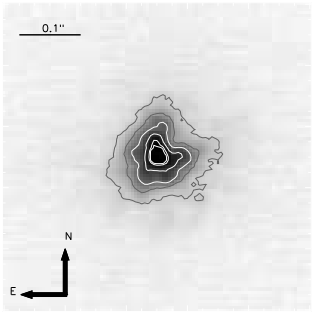
(viii) *2MASS J0300+2130*.



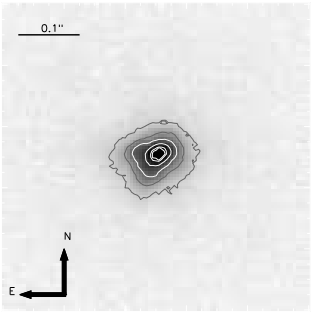
(ix) *2MASS J0302+1358*.



(x) *2MASS J0344+0110*.

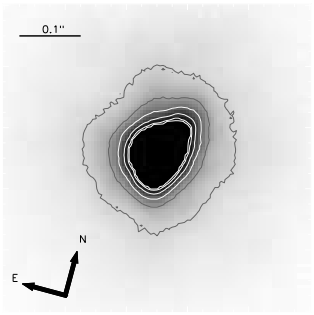


(xi) *SDSS J0351+4810*.

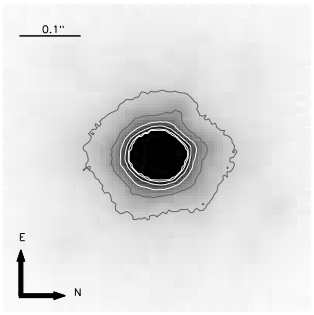


(xii) *HTY J0429+1535*.

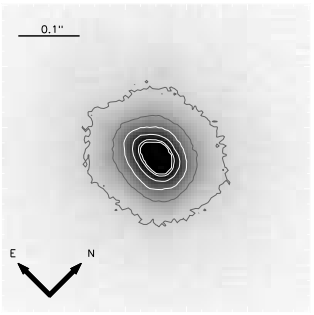
Fig. 2.— Keck NIRC2 LGS-AO images in the H band of all targets. Contours are drawn at 20, 40, 60, 80, 95 and 99% of the image minimum.



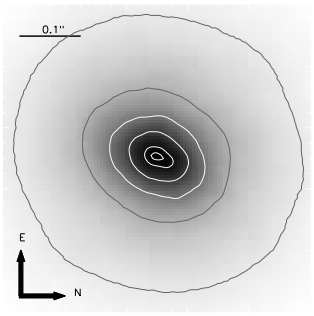
(i) *2MASS J0443-3202.*



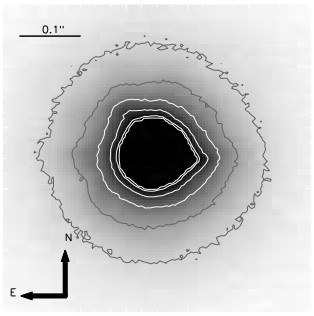
(ii) *2MASS J0518−2828.*



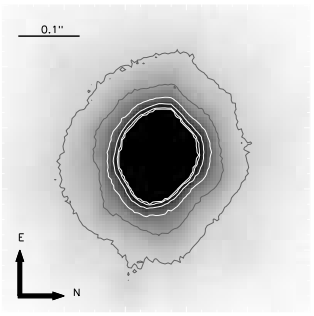
(iii) *WISE J0528+0901.*



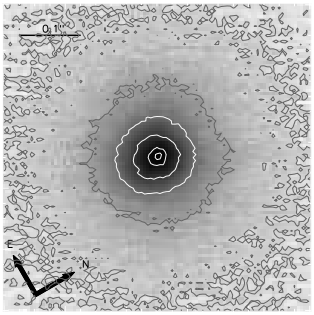
(iv) *WISE J0720-0846.*



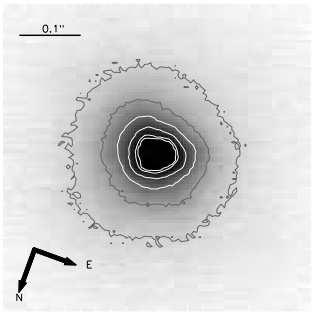
(v) *SDSS J0758+3247.*



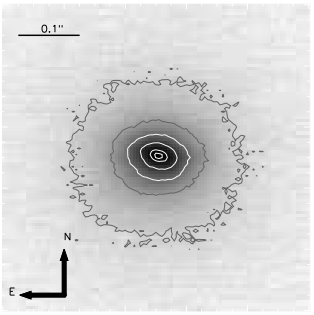
(vi) *SDSS J0805+4812.*



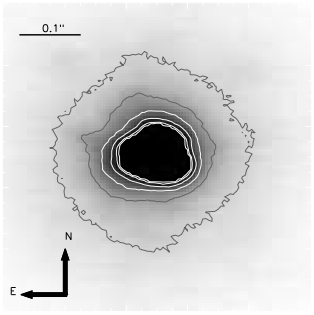
(vii) *SDSS J0931+0327.*



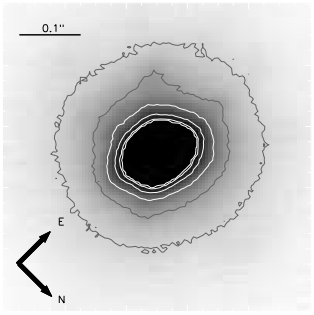
(viii) *2MASS J0949−1545.*



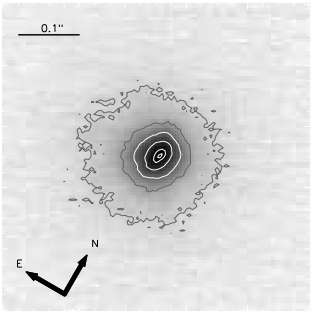
(ix) *SDSS J1033+4005.*



(x) *2MASS J1106+2754.*

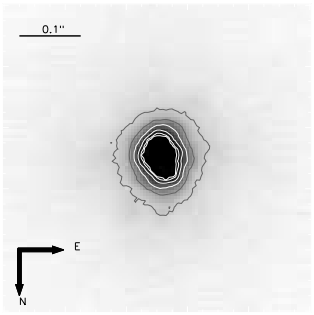


(xi) *SDSS J1121+4332.*

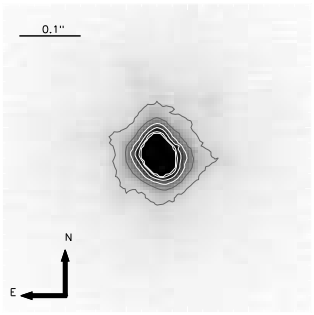


(xii) *2MASS J1150+0520.*

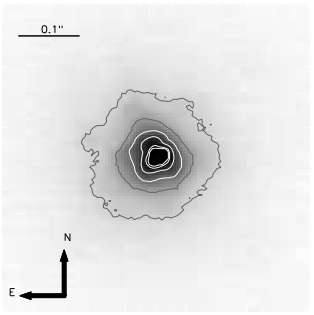
Fig. 2.— *(Continued.)*



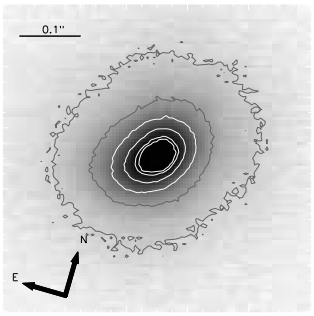
(i) *2MASS J1158+0435.*



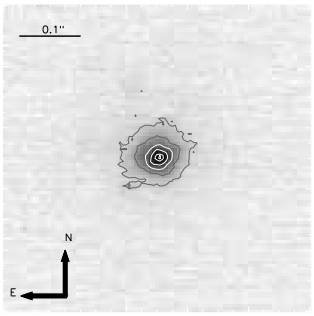
(ii) *SDSS J1206+2813.*



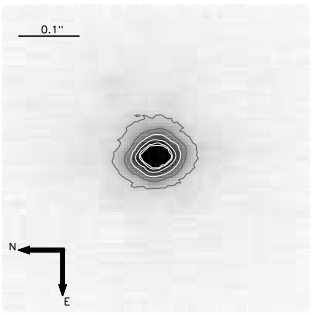
(iii) *2MASS J1209-1004.*



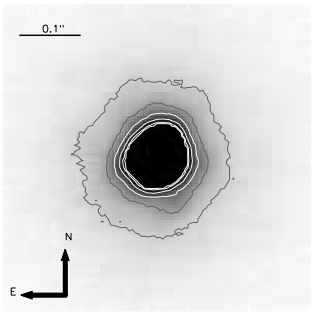
(iv) *ULAS J1326+1200.*



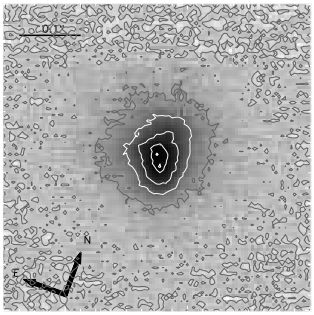
(v) *2MASS J1414+0107.*



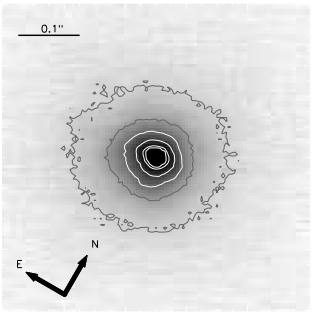
(vi) *2MASS J1428+5923.*



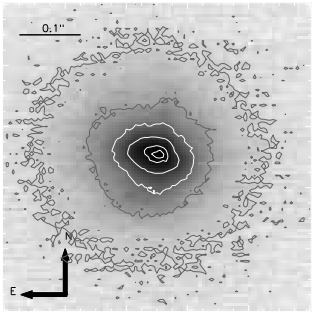
(vii) *SDSS J1435+1129.*



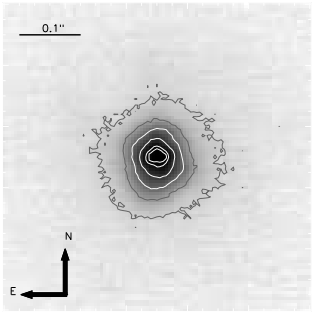
(viii) *SDSS J1516+3053.*



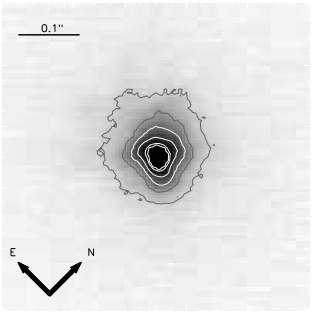
(ix) *SDSS J1547+0336.*



(x) *2MASS J1707+4301.*

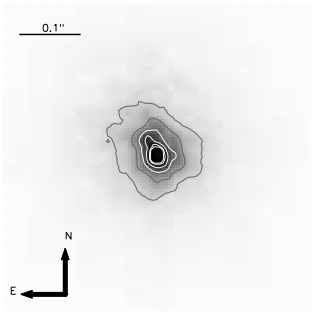


(xi) *2MASS J1711+2232.*

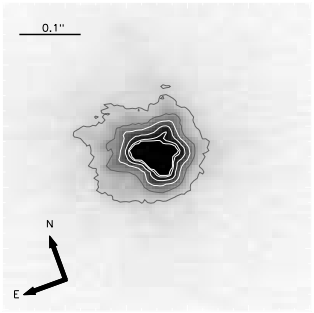


(xii) *2MASS J1721+3344.*

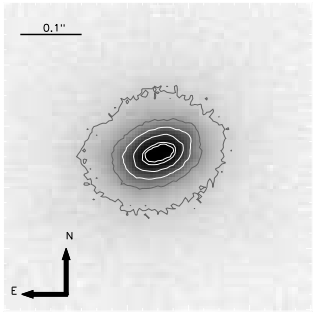
Fig. 2.— *(Continued.)*



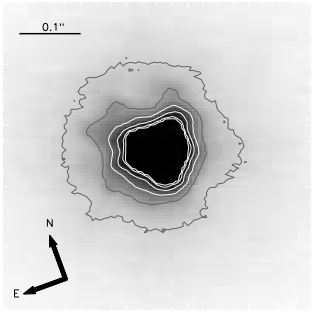
(i) *2MASS J1733−1654.*



(ii) *2MASS J2002-0521.*



(iii) *2MASS J2126+7617.*



(iv) *2MASS J2149+0603.*

Fig. 2.— *(Continued.)*

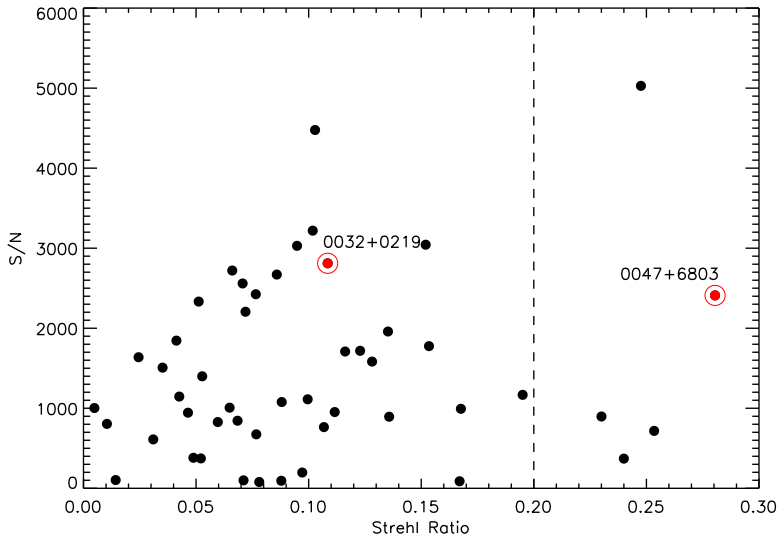


Fig. 3.— Strehl ratio vs. signal-to-noise ratio of all H band observations (black dots). The two representative sources used in the empirical sensitivity curves are marked in red. The three groups are separated by the dashed lines. See Table 1 for the list of objects.

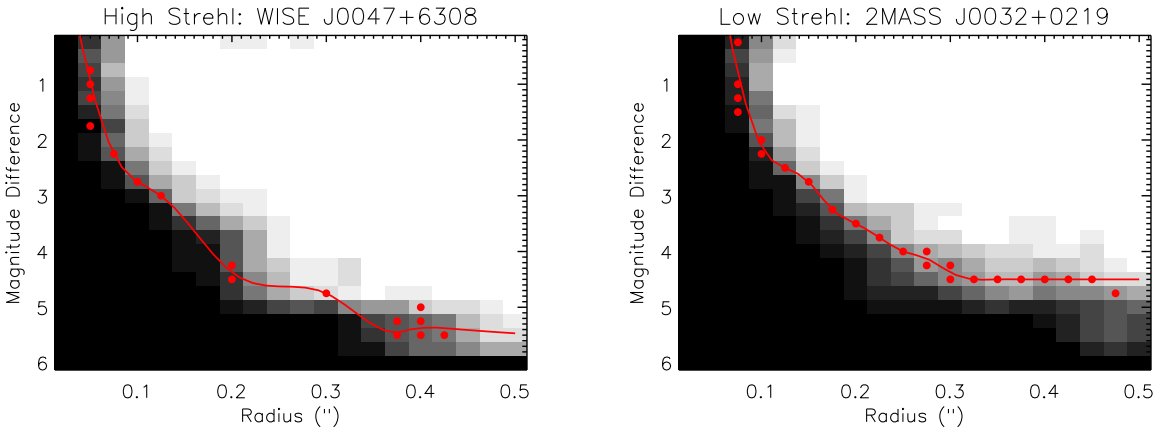


Fig. 4.— Empirical sensitivity curves from simulated binaries for two representative sources based on their Strehl and signal-to-noise ratios (see Table 1). The red line delimits the detections of secondaries (white) from non-detections (black).

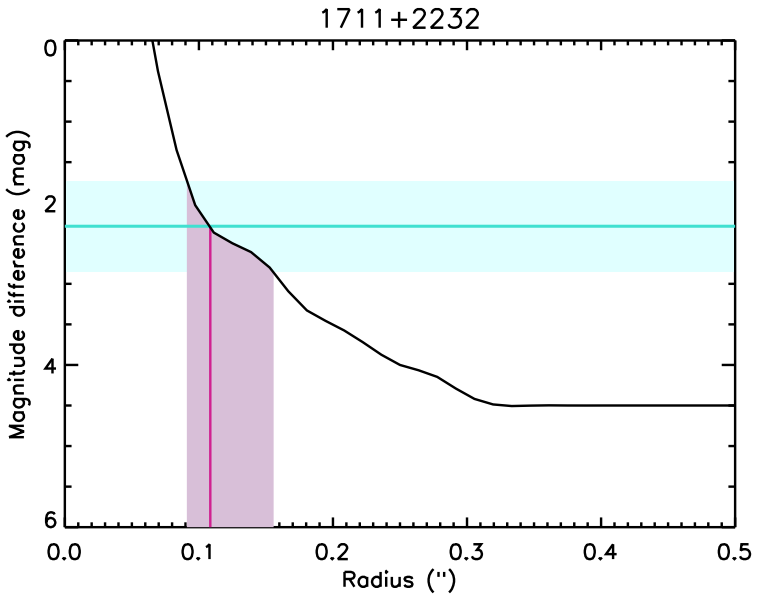


Fig. 5.— Example separation constraint for 2MASS J1711+2232. Given the empirical sensitivity curve for its Strehl ratio vs. S/N group (low Strehl-low S/N, representative source: 2MASS J0032+0219) in black, and the estimated magnitude difference in cyan (uncertainties are shown as the shaded region), we can set an upper limit for an undetected secondary at the intersection (magenta line). The values for the separation constraints for all observations are reported in Table 3.

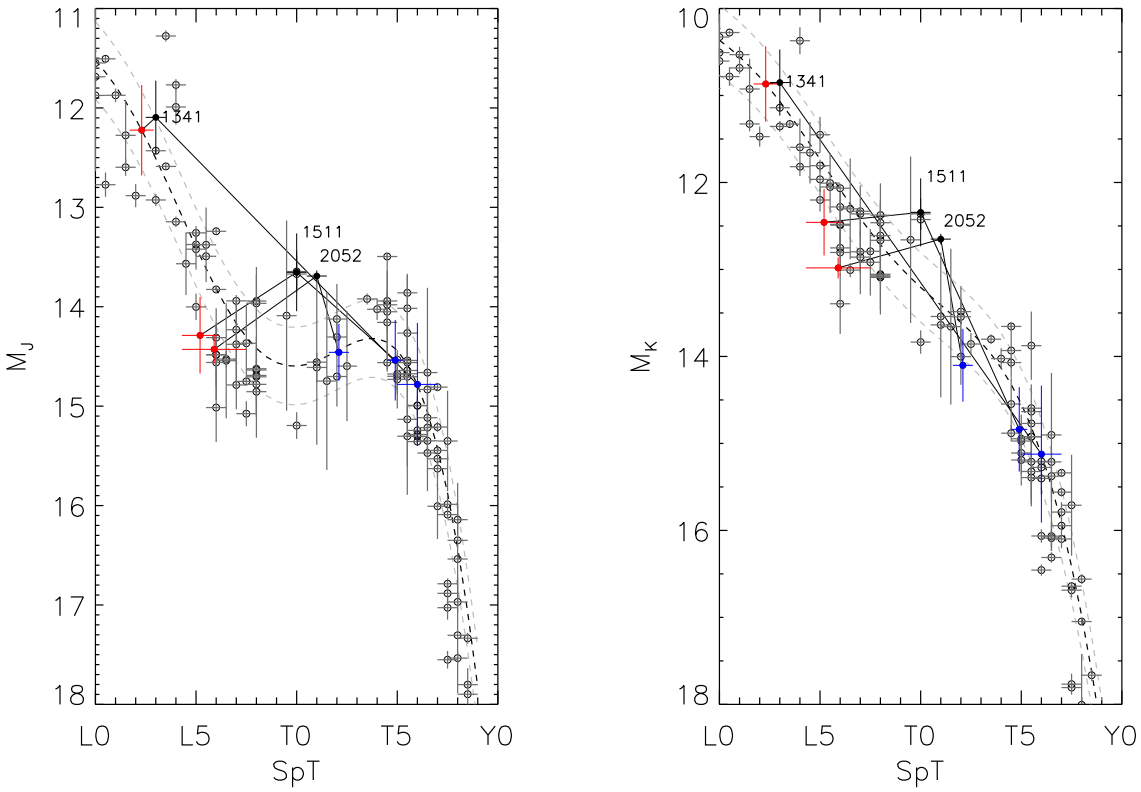


Fig. 6.— Absolute magnitudes in J and K_s for the three resolved binaries (black dots) and the Dupuy & Liu (2012) parallax sample (grey circles) shown with the Dupuy & Liu (2012) spectral type to absolute magnitude relation (black dashed line) and its 1-σ outliers (grey dashed lines). Only SDSS J1511+0607 and SDSS J2052−1609 have parallaxes reported in the literature. The three binaries are split into component spectral types, where the primaries for the two objects with parallaxes lie on the faint end of the absolute magnitude relation for their spectral type (red dots) , and the secondaries (blue dots) are all within 1-σ from the relation.

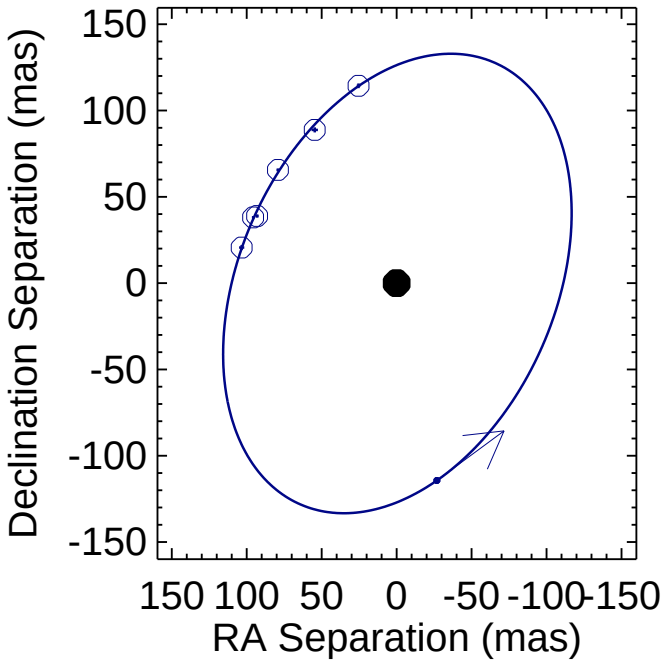


Fig. 7.— Visual orbit of SDSS J2052−1609AB based on MCMC analysis of separation measurements reported here and in Stumpf et al. (2011, open circles). The orbital motion of the secondary (blue line) relative to the primary (black dot at the origin) is shown projected on the sky, with the arrow indicating the direction of orbital motion at periaps ($M = 0°$). Error bars are plotted but indiscernible on this scale.

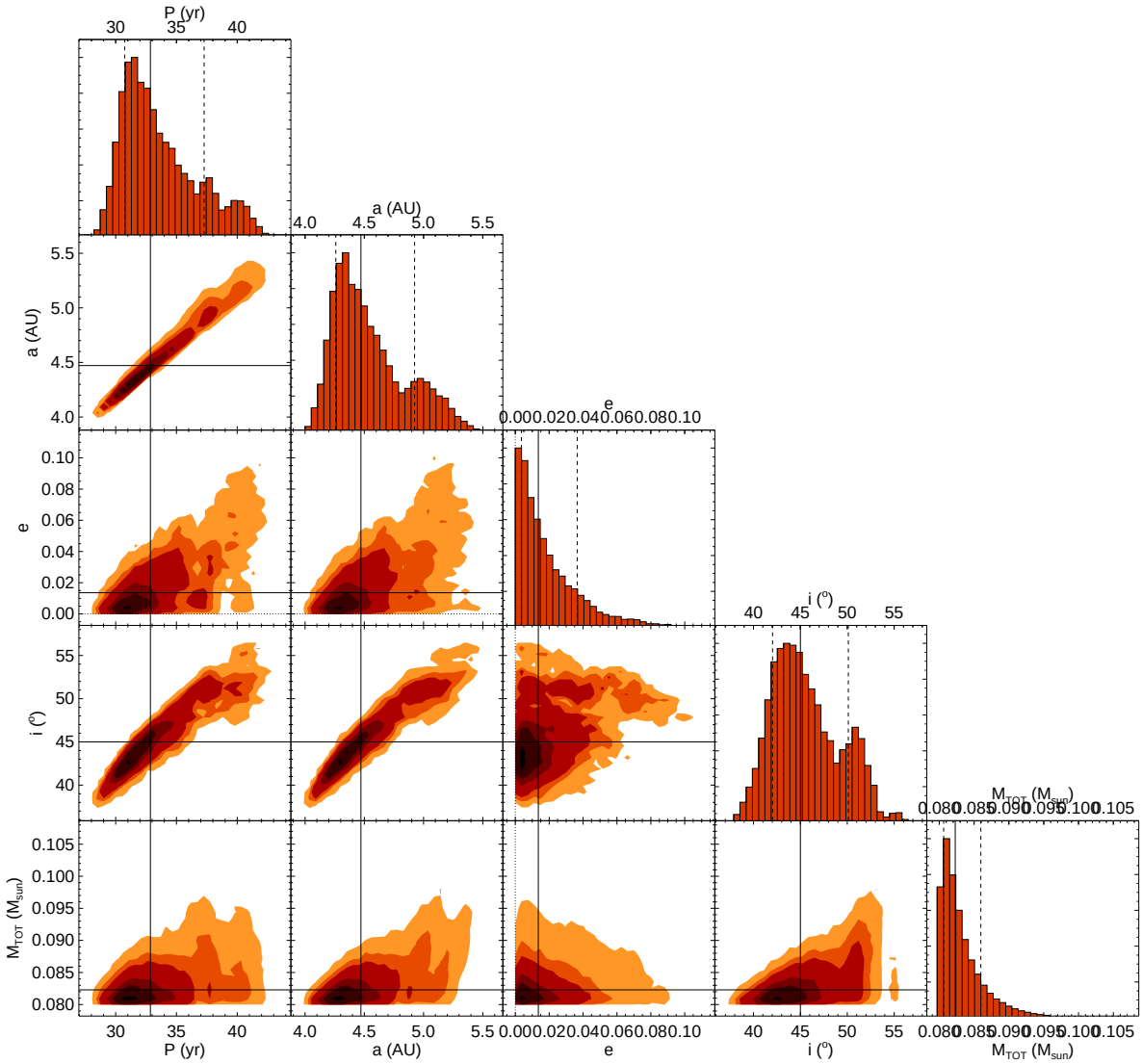
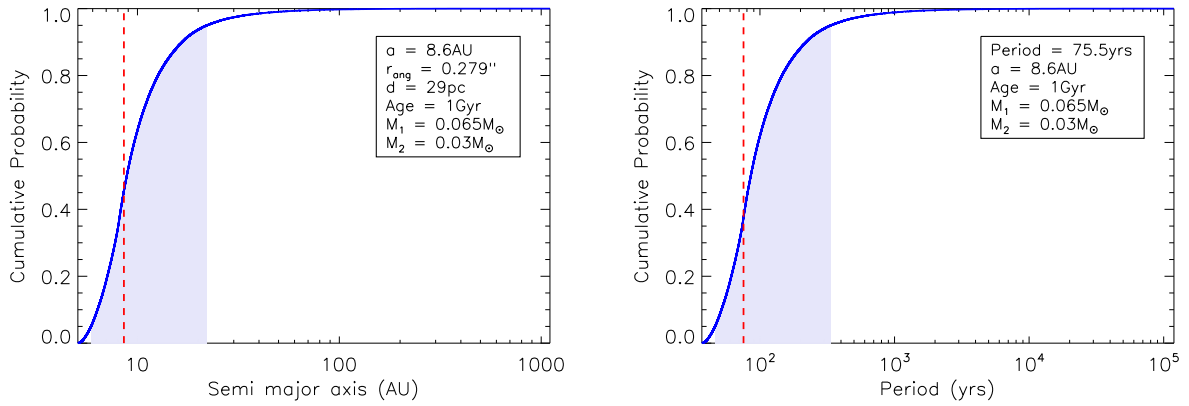
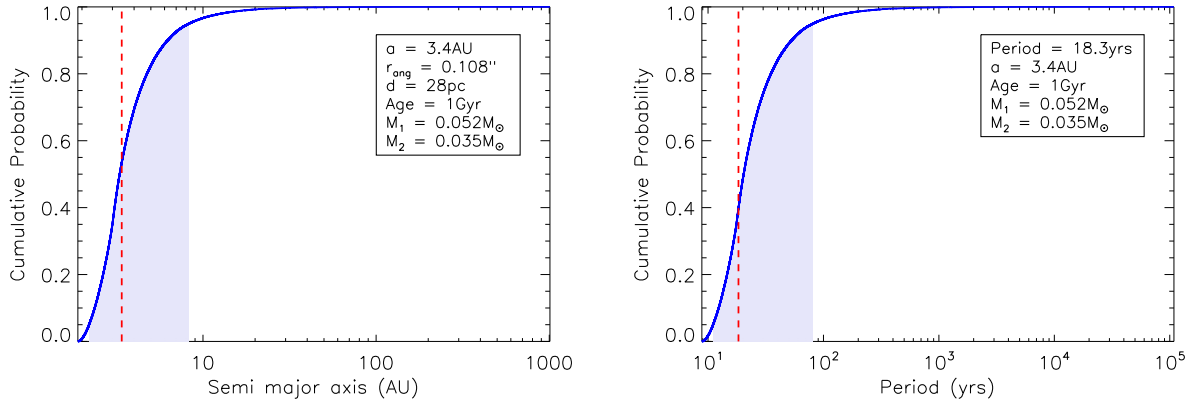


Fig. 8.— Parameter distributions and correlations (triangle plot) for period (P), semi-major axis (a), eccentricity (e), inclination (i), and total system mass (M_{tot}) based on our MCMC orbital analysis of SDSS J2052−1609AB. Contour plots show χ^2 distributions as a function of parameter pairs, highlighting correlations. Normalized histograms at the ends of rows are marginalized over all other parameters. Median values are indicated by solid lines in all panels, and 16% and 84% quantiles are indicated by dashed lines in the histograms.



(a) *2MASS J1341−3052.*



(b) *SDSS J1511+0607.*

Fig. 9.— Cumulative probability distribution of possible semi-major axes and periods for two of the resolved sources from a Monte Carlo simulation for an age of 1Gyr, using one single observation for projected separation from the LGS-AO images in each case. The simulation parameters are shown on the box in the upper right corner. The most likely semi-major axis and period is represented by the dotted red line. The shaded regions indicate the central 68% ($\pm 1\sigma$ equivalent) of data points.